

RESEARCH

Open Access



Integrative multi-omics analysis reveals the LncRNA 60967.1–PLCD4–ATRA axis as a key regulator of colorectal cancer progression and immune response

Yiyi Chen^{1†}, Ningning Zhao^{3,4*†}, Lingna Xu^{1†}, Xiya Jia¹, Fang Liu^{3,4}, Jian Huang^{3,4}, Xuhua Li^{3,4}, Yunfei Wang⁵, Chuanxi Lai¹, Yanbin Shen¹, Fei Wang¹, Yiming Lv¹, Xuefeng Huang¹, Fan Zhang^{3,4*}, Hongcang Gu^{2,3,4*} and Sheng Dai^{1,2*}

Abstract

Colorectal cancer (CRC) is a major global health concern, characterized by high morbidity and mortality rates. CRC progression involves intricate molecular networks that remain incompletely understood. In this study, we conducted an integrative multi-omics analysis of transcriptomic, proteomic, and metabolomic profiles from CRC tissues and matched normal adjacent tissues (NATs). Our analysis revealed 1,394 differentially expressed long non-coding RNAs (lncRNAs), 2,788 genes, 548 proteins, and 91 metabolites. A significant interaction network comprising 22 lncRNAs, 14 mRNAs/proteins, and 9 metabolites was identified, among which lncRNA 60967.1 emerged as a pivotal regulator. Functional validation demonstrated that lncRNA 60967.1 is markedly downregulated in CRC cell lines and patient tissues. Overexpression of lncRNA 60967.1 restored expression of the tumor suppressor PLCD4 and increased levels of all-trans retinoic acid (ATRA). This modulation enhanced IFN- γ -induced apoptosis and increased expression of the IFN- γ receptor subunit IFNGR1, thereby partially reversing IFN- γ resistance. In murine models, lncRNA 60967.1 overexpression promoted immune cell infiltration and synergized with anti-PD-1 therapy to inhibit tumor growth. Collectively, our findings uncover a novel lncRNA-mRNA/protein-metabolite network, the lncRNA 60967.1-PLCD4-ATRA axis, that plays a critical role in CRC progression and immune modulation, offering promising therapeutic targets for improved treatment efficacy.

[†]Yiyi Chen, Ningning Zhao, and Lingna Xu contributed equally to the work.

*Correspondence:

Ningning Zhao
nnzhao@cmpt.ac.cn
Fan Zhang
fzhang@cmpt.ac.cn
Hongcang Gu
gu_hongcang@cmpt.ac.cn
Sheng Dai
daimd@zju.edu.cn

Full list of author information is available at the end of the article



© The Author(s) 2025. **Open Access** This article is licensed under a Creative Commons Attribution-NonCommercial-NoDerivatives 4.0 International License, which permits any non-commercial use, sharing, distribution and reproduction in any medium or format, as long as you give appropriate credit to the original author(s) and the source, provide a link to the Creative Commons licence, and indicate if you modified the licensed material. You do not have permission under this licence to share adapted material derived from this article or parts of it. The images or other third party material in this article are included in the article's Creative Commons licence, unless indicated otherwise in a credit line to the material. If material is not included in the article's Creative Commons licence and your intended use is not permitted by statutory regulation or exceeds the permitted use, you will need to obtain permission directly from the copyright holder. To view a copy of this licence, visit <http://creativecommons.org/licenses/by-nc-nd/4.0/>.

Significance

Colorectal cancer (CRC) is characterized by substantial genetic and epigenetic heterogeneity, underscoring the need for novel therapeutic targets. While immunotherapy has led to significant advancements in cancer treatment, approximately 85% of CRC patients exhibit resistance due to different genetic and epigenetic features. Multi-omics approaches, which integrate data across genomic, proteomic, and metabolomic layers, have emerged as powerful tools for elucidating disease mechanisms. In this study, we conducted multi-omics analyses on tumor and adjacent normal tissues from 13 CRC patients. Complementary *in vitro* and *in vivo* experiments demonstrated that lncRNA 60967.1 regulates the PLCD4/ATRA axis and modulates the immune response to anti-PD-1 therapy, thereby promoting CRC progression. Our findings reveal a novel regulatory network involving lncRNA, PLCD4, and ATRA, providing a potential new target for CRC therapy.

Keywords Colorectal cancer, Multi-omics, lncRNAs, Tumor microenvironment, Immunity

Introduction

Colorectal cancer (CRC) ranks as the third most frequently diagnosed cancer worldwide and is the second leading cause of cancer-related deaths [1–3]. While the five-year overall survival rate for early-stage localized CRC is high, exceeding 90%, the prognosis significantly worsens for metastatic CRC (mCRC), where the five-year survival rate drops to around 14% [4, 5]. Unfortunately, up to 25% of CRC cases are already metastatic at diagnosis, and about 50% of localized CRC patients eventually develop mCRC. Conventional therapies such as surgery, chemotherapy, and radiotherapy offer limited long-term survival benefits [6, 7]. The heterogeneity of CRC, characterized by complex genetic and epigenetic alterations, necessitates the identification of novel therapeutic targets to improve patient outcomes [8, 9].

In recent years, immunotherapy has transformed the treatment landscape for various cancers, including CRC. Immune checkpoint inhibitors (ICI), such as pembrolizumab and nivolumab, have shown promising results, especially in CRC patients with high microsatellite instability (MSI-H) or deficient mismatch repair (dMMR) tumors, which account for approximately 15% of stage I–III CRC cases and 3–6% of stage IV CRC patients [10]. MSI-H/dMMR tumors harbor numerous somatic mutations encoding neoantigens, making them more responsive to immune checkpoint inhibitors [3]. However, approximately 95% of mCRC patients are microsatellite stable (MSS) or mismatch repair-proficient (MMRp), rendering them resistant to immunotherapy [11]. This underscores the need for further investigation into the molecular mechanisms regulating immune responses in CRC.

Integrative multi-omics data analysis has emerged as a powerful approach to uncover the molecular networks that drive cancer progression [12, 13]. By integrating high-throughput datasets such as transcriptomics, proteomics, and metabolomics, this approach provides a more comprehensive understanding of cancer pathogenesis than single omics layers alone [14, 15]. Multi-omics

analysis enables the classification of disease subtypes, identification of predictive biomarkers, and provides insights into the molecular mechanisms underlying diseases. For example, one study profiled 34 CRC cell lines using genomic, transcriptomic and proteomic analyses and confirmed that these cell lines accurately recapitulate the genomic profiles of primary carcinomas and can be stratified into distinct molecular subtypes [16]. Similarly, Takei and colleagues conducted a multiomic characterization of MSS/MMRp CRC tumors from patients treated with ICI combinations, identifying molecular features such as upregulated epithelial-mesenchymal transition and G2M checkpoint pathways, POLE mutations, and tumor microenvironment factors as predictive biomarkers for treatment response, which could aid in the development of biomarkers for ICI therapy [17]. In a large cohort study involving 100,204 CRC cases and 154,587 controls, Fernandez-Rozadilla and colleagues identified 50 novel risk association markers. Integrative genomic, transcriptomic, and methylomic analyses revealed 53 additional associations and 155 effector genes linked to CRC risk, many of which were previously unreported [18].

To investigate the molecular mechanisms driving CRC progression, we conducted a multi-omics analysis integrating transcriptomics, proteomics, and metabolomics of CRC tissues and matched normal adjacent tissues (NATs) from 13 patients. Although large-scale databases like The Cancer Genome Atlas (TCGA) provide a wealth of multi-omics data for CRC with a substantial sample size, TCGA primarily employs Reverse Phase Protein Array (RPPA) for proteomics analysis and lacks data on non-coding RNAs. Moreover, we incorporated metabolomics analysis, providing insights into metabolic changes in CRC, which is not covered in TCGA's datasets. In contrast, the uniqueness of this study lies in its focus on non-coding RNAs, combined with mass spectrometry-based proteomics and metabolomics integration. Additionally, the use of consistent samples across all omics data in this study allows for a clearer understanding of the interactions between molecules at different layers [19, 20].

Through hierarchical clustering and network analysis, we identified differentially expressed lncRNA (DELncs), genes (DEGs), proteins (DEPs), and metabolites (DEMs). Our analysis then examined the interactions between lncRNAs, mRNAs/proteins, and metabolites, revealing key lncRNAs strongly correlated with gene expression and metabolic alterations. Further validation using *in vitro* and *in vivo* experiments demonstrated the role of lncRNA 60967.1 in modulating the PLCD4/ATRA axis and anti-PD-1 therapy, influencing immune responses and impacting CRC progression.

Materials and methods

Sample collection

Thirteen pairs of human CRC tissue samples and matched NATs were collected immediately after surgical resection at Sir Run Run Shaw Hospital, Hangzhou, China (Supplementary Table S1). Sample collection adhered to Institutional Review Board (IRB) guidelines and was approved by the Ethics Committee (20211204-30). Pathological examination confirmed that all specimens were CRC. Patients were excluded if they had received prior treatment, had other tumors, incomplete clinical data, coexisting blood disorders, or recent antibiotic use.

Multi-omics sample preparation and data analysis

Total RNA was extracted from CRC tissues and NATs using Trizol Reagent (Invitrogen Life Technologies). To assess RNA quality, concentration, and integrity, we used the Thermo Scientific NanoDrop spectrophotometer. Subsequently, ribosomal RNA (rRNA) was removed from the total RNA using the Epicentre Ribo-Zero rRNA Removal Kit (Human/Mouse/Rat), following the manufacturer's protocol. Next, first-strand cDNA was synthesized using random oligonucleotides as primers, and RNA degradation was carried out with RNase H. For the second strand, DNA polymerase I was used to synthesize cDNA, with dTTP substituted by dUTP. Afterward, the cDNA was purified, end-repaired, A-tailed, and adapter-ligated. To eliminate the second cDNA strand containing uracil (U), the USER enzyme (NEB, USA) was added.

To enrich the synthesized double-stranded DNA, a 15-cycle PCR amplification was performed using the Illumina PCR Primer Cocktail. The PCR products were then purified with the AMPure XP Bead-Based Reagent (Beckman Coulter, Beverly, CA, USA). The quality and quantity of the library was assessed using the Agilent High Sensitivity DNA Assay on the Agilent 2100 Bioanalyzer System and then sequenced on the Illumina NovaSeq 6000 platform.

For gene expression analysis, we used HTSeq (v0.9.1) to calculate the read count values for each gene. These values were then normalized using fragments per kilobase

of transcript per million mapped reads (FPKM). In order to assemble the transcripts, we utilized StringTie (v2.2.1) along with Hisat2 (v2.1.0) alignment results. Candidate long non-coding RNAs (lncRNAs) were identified from the assembled transcripts based on characteristic splicing patterns and structural features typical of lncRNAs. To further validate the non-coding nature of the transcripts, we used three software tools-PLEK (v1.2), CNCI (v1.0), and Pfamscan (v1.6.4)-to predict their coding potential. Only those transcripts for which all three tools indicated non-coding characteristics were classified as lncRNAs. RNA sequencing was carried out by Suzhou Panomics Biopharmaceutical Technology, with transcript quantification performed using HTSeq (v0.9.1). DEGs were identified using DESeq, considering both q-values and fold changes [21]. Finally, detailed information regarding the HE staining results and tumor purity, assessed by pathologists, can be found in Supplementary Fig. S1.

For proteomic analysis, CRC tissues were homogenized using the MP FastPrep-24 instrument and lysed in SDT buffer (4% SDS, 100 mM DTT, 150 mM Tris-HCl, pH 8.0), supplemented with an appropriate amount of Protease and Phosphatase Inhibitor Cocktail (EDTA-Free, 10x in ddH₂O). The protein concentration was normalized, and ultrafiltration was employed to remove detergents, DTT, and other small molecules. To block reduced cysteine residues, iodoacetamide was added, and the reaction was incubated in the dark for 30 min. The samples were then washed with UA buffer (8 M urea, 150 mM Tris-HCl, pH 8.0), followed by NH₄HCO₃ buffer to further clean the preparations. Subsequently, trypsin (Promega) was added to the samples, and protein digestion was carried out overnight at 37 °C. The resulting peptides were collected and prepared for fractionation using the Scientific Pierce high-pH reversed-phase kit. Retention time correction was performed using iRT-Kits (Biognosys) according to the manufacturer's guidelines. For Data-Dependent Acquisition (DDA) library generation, all peptide fractions were injected into a Thermo Scientific Q Exactive HF-X mass spectrometer connected to a Thermo Scientific Easy nLC 1200 chromatography system. The DDA library data were searched against the FASTA sequence database using Spectronaut (v14.4.200727.47784, Biognosys) or Data-Independent Acquisition (DIA), peptides from each sample were analyzed by liquid chromatography-tandem mass spectrometry (LC-MS/MS). A spectral library was generated by importing the original raw files and DDA search results into Spectronaut Pulsar X (v12.0.20491.4, Biognosys). The DIA data were processed in Spectronaut, referencing the constructed spectral library to ensure accurate peptide identification and quantification.

DEPs were identified using a combination of statistical tests. A t-test was applied for normally distributed data,

while the Wilcoxon rank-sum test was used for non-normally distributed data. Principal component analysis (PCA) was performed to assess data variability, while Pearson correlation and weighted gene co-expression network analysis (WGCNA) were used to explore the relationships between mRNA and protein expression levels [22].

For metabolomics analysis, the liquid chromatography (LC) system (Thermo Vanquish) was coupled with a mass spectrometer (MS) (Thermo QE-HF-X). Initially, the sample was precisely weighed, and an extraction mixture composed of 75% methanol and a 9:1 chloroform-to-water ratio (25%) was added. Steel beads were introduced, and the sample was homogenized using a high-throughput tissue homogenizer at 50 Hz for 60 s. The mixture was then subjected to ultrasonication at room temperature for 30 min, followed by a 30-minute incubation on ice. After centrifugation at 12,000 rpm for 10 min at 4 °C, the supernatant (approximately 850 µL) was collected and transferred into a 2 mL centrifuge tube. The solution was dried using a vacuum concentrator, and reconstitution was performed with 50% acetonitrile solution containing 4 ppm 2-chlorophenylalanine. The solution was filtered through a 0.22 µm membrane into a detection vial. To create a quality control (QC) sample, 20 µL from each sample was pooled. LC-MS analysis was subsequently performed on the remaining test samples.

Metabolomics data analysis was conducted using OmicStudio (<https://www.omicstudio.cn>) and OECloud (<https://cloud.oebiotech.com>) platforms [23]. Partial least squares discriminant analysis (PLS-DA) was used to generate the PLS score plot and model validation plot in R (v4.0.3). A t-test was employed to identify differentially expressed metabolites (DEMs), followed by functional pathway enrichment analysis using MetaboAnalyst (27). Stamp plot analysis was generated using OmicStudio, and receiver operating characteristic (ROC) curves were constructed to assess the potential of DEMs for CRC identification. Pearson correlation was applied to explore the relationships between DEMs and mRNAs/proteins.

Cell lines and reagents

CRC cell lines, including DLD1, HCT8, HCT116, and SW480, were obtained from Prosai, while NCM460 and MC38 cell lines were sourced from Warner Bio. All cell lines were cultured in either DMEM or RPMI-1640 medium, each supplemented with 10% fetal bovine serum (FBS) and 1% penicillin/streptomycin. Authentication of all cell lines used in this study was performed through STR (short tandem repeat) profiling to ensure their identity and integrity.

Isolation of RNA, reverse transcription, and quantitative RT-PCR (qRT-PCR) analysis.

Total RNA was isolated from samples using TRIzol reagent (Invitrogen), according to the manufacturer's instructions. cDNA was synthesized from 1 µg of RNA using the PrimeScript RT Master Mix (Takara). qRT-PCR was performed with TB Green Premix Ex Taq II (Takara) following the manufacturer's protocols. The amplification conditions were optimized for each target gene. Primer sequences used in this study are provided in Supplementary Table S2.

Western blot analysis

Cells were lysed in RIPA buffer (Sigma-Aldrich) containing protease inhibitors to extract total protein. Protein samples were separated by SDS-PAGE and transferred to PVDF membranes (Millipore). Membranes were blocked with 2.5% nonfat milk and incubated overnight at 4 °C with primary antibodies. After washing, membranes were incubated with appropriate secondary antibodies. Protein bands were detected using an enhanced chemiluminescence (ECL) detection system (Thermo Fisher Scientific). Details of the antibodies used, including their sources and dilutions, are provided in Supplementary Table S3.

Hematoxylin and Eosin (H&E) and immunohistochemistry (IHC) analysis

CRC cell lines (DLD1, HCT8, SW480) and normal colon cells (NCM460) were fixed in 4% paraformaldehyde. The fixed cells were subjected to standard H&E staining or IHC staining using the SP Rabbit & Mouse HRP Kit (CW2069S, Beijing, China) with hematoxylin as a counterstain. Primary antibodies against PLCD4, CD4, and CD8 were applied according to the manufacturer's instructions. Antibody details, including dilution factors, are provided in Supplementary Table S3. For IHC analysis, the staining intensity and the percentage of positively stained cells were evaluated semi-quantitatively. The percentage of positive cells was categorized into the following four grades: 0 (<5%), 1 (6–25%), 2 (26–50%), 3 (51–75%), and 4 (>75%). The intensity of staining was classified into four levels: 0 (negative), 1 (weak), 2 (moderate), and 3 (strong). For each tissue section, ten high-magnification fields (x400) were analyzed, and the average score was calculated based on the intensity and percentage of positive cells [24, 25].

Enzyme-linked immunosorbent assay (ELISA)

ELISA assays were performed using culture supernatants from cell cultures, and detection was carried out using commercially available kits from Shanghai Enzyme-linked Biotechnology Co., Ltd (Shanghai). For lentiviral transfection, cells were seeded at a density of $3\text{--}5 \times 10^4$

cells/mL in 12-well plates. When cells reached 30–50% confluence, polybrene (7 µg/mL) was added to enhance viral infection, and cells were infected with lentiviral particles from General Biology Anhui Co., Ltd. Transfection efficiency was assessed 72 h post-infection by measuring the expression of the transgene.

RNA fluorescence in situ hybridization (RNA FISH)

For RNA FISH (GimaGen), cells were seeded on confocal dishes and fixed with 4% paraformaldehyde. After fixation, the cells were blocked to reduce non-specific binding. Hybridization with specific probes was performed overnight at 37 °C. Nuclei were counterstained with DAPI. Images were captured using a laser scanning confocal microscope to visualize RNA localization and expression.

Analysis of PLCD4 expression and tumor microenvironment (TME) infiltration patterns

The relationship between PLCD4 expression and TME infiltration patterns in CRC was systematically investigated using data from the TCGA CRC cohort. Standardized gene expression profiles (TPM) for both TCGA Colon Adenocarcinoma (TCGA-COAD) and TCGA Rectal Adenocarcinoma (TCGA-READ) were downloaded via the “GDCquery” function of the “TCGAbiolinks” R package. Prior to merging the mRNA expression matrices of TCGA-COAD and TCGA-READ, potential batch effects were assessed using the “draw_pca” function of the “tinyarray” R package. No significant batch effects were detected (Supplementary Fig. S7A). The two datasets were then combined, resulting in a unified mRNA expression matrix for the TCGA-CRC cohort, which included 650 CRC samples.

To assess the TME, the Estimation of Stromal and Immune Cells in Malignant Tumors Using Expression Data (ESTIMATE) algorithm (1) was applied to calculate the ImmuneScore, StromalScore, and Tumor Purity for each sample. Pearson’s correlation analysis was performed to examine the relationship between PLCD4 mRNA expression levels ($\log_2(\text{TPM} + 1)$) and these scores. Additionally, to validate the findings from the ESTIMATE algorithm, the xCell algorithm (2) was employed using the “xCell” R package. The xCell-based microenvironment score represents the sum of all immune and stromal cell types within the TME.

RNA immunoprecipitation (RIP) assay for PLCD4-RNA complexes

RIP was performed using the RNA Immunoprecipitation Kit (Cat. No. P0102, Genesee, Guangzhou) according to the manufacturer’s instructions. NCM460 cells were collected and lysed, and 100 µL of the lysate was saved as the input sample. To capture the PLCD4-RNA complex,

human PLCD4 antibody (30133-1-AP, Proteintech) and IgG antibody were incubated with Protein A+G beads overnight at 4 °C. The immunoprecipitated RNA-protein complexes were then used for downstream analysis, including qRT-PCR to quantify RNA levels and Western blot analysis to detect protein expression.

In vivo tumor xenograft and treatment models

Immunocompetent and nude BALB/c mice (4–6 weeks old) were obtained from Jiangsu Jicui Yaokang Biotechnology Co., Ltd. All animal experiments were approved by the Institutional Animal Care and Use Committee (IACUC) of the respective institutions. For the human CRC xenograft model, 6-week-old BALB/c nude mice were subcutaneously injected with 5×10^6 HCT116 cells transfected with either a control or PLCD4-overexpressing vector ($n=6$ per group). Tumor size was measured every 2–3 days starting on day 5, and tumor volume was calculated using the formula: $(\text{length} \times \text{width}^2)/2$.

For the mouse CRC model, 5×10^6 CT26 cells, transfected with either GFP or lncRNA 60967.1 vectors, were injected subcutaneously. Tumor size was measured every 4 days using the same formula. After 20 days, tumors were harvested, weighed, and embedded in paraffin for further analysis.

For PD-1 and lncRNA-targeting treatment, 250 µg of anti-PD-1 monoclonal antibody (RMP1-14, BioXCell) was administered via intraperitoneal injection once a week, starting 5 days after the establishment of the CT26 mouse model.

Statistical analysis and data interpretation

Statistical significance was assessed using GraphPad Prism 8 software and the R programming language. All assays were performed in triplicate, with results presented as the mean \pm SEM unless otherwise indicated. *P*-values were calculated using two-tailed Student’s *t*-tests. Pearson’s correlation coefficient was used for correlation analysis to assess the relationship between mRNA and protein module eigengenes and traits, with a correlation coefficient threshold of ≥ 0.3 and a *p*-value < 0.05 for selection. We performed WGCNA on mRNA and proteins, setting the power value to 1 for mRNA and 14 for proteins based on the distribution and connectivity of the scale-free network. PLS-DA was conducted in R (v4.0.3) to evaluate the PLS score and model validation plots. ROC analysis of metabolites was performed using OmicStudio or OECloud, with *p*-values < 0.05 considered statistically significant. ELISA data were similarly analyzed using two-tailed Student’s *t*-tests. Further details on statistical methods are provided in the figure captions.

Results
Integrative multi-omics analysis reveals novel lncRNA-mRNA/protein-metabolite crosstalk driving CRC progression

To investigate the mechanisms underlying CRC progression, we performed a comprehensive multi-omics analysis, including transcriptomics, proteomics, and metabolomics, on CRC tissues and matched NATs from 13 patients. We analyzed and validated datasets consisting of 26 transcriptomes, 22 proteomes (11 patients), and

66 metabolomes (11 patients, triplicate per sample). Initially, 2,788 DEGs and 818 DEPs were identified (Fig. 1A and B). Unsupervised hierarchical clustering of mRNA and protein expression data revealed distinct expression patterns between CRC and NAT samples (Fig. 1C and D). By integrating transcriptomic and proteomic data, we identified 106 upregulated and 124 downregulated genes in CRCs compared to NATs, demonstrating a consistent expression trend between mRNA and protein expression (Fig. 1E). After excluding genes with low and unstable

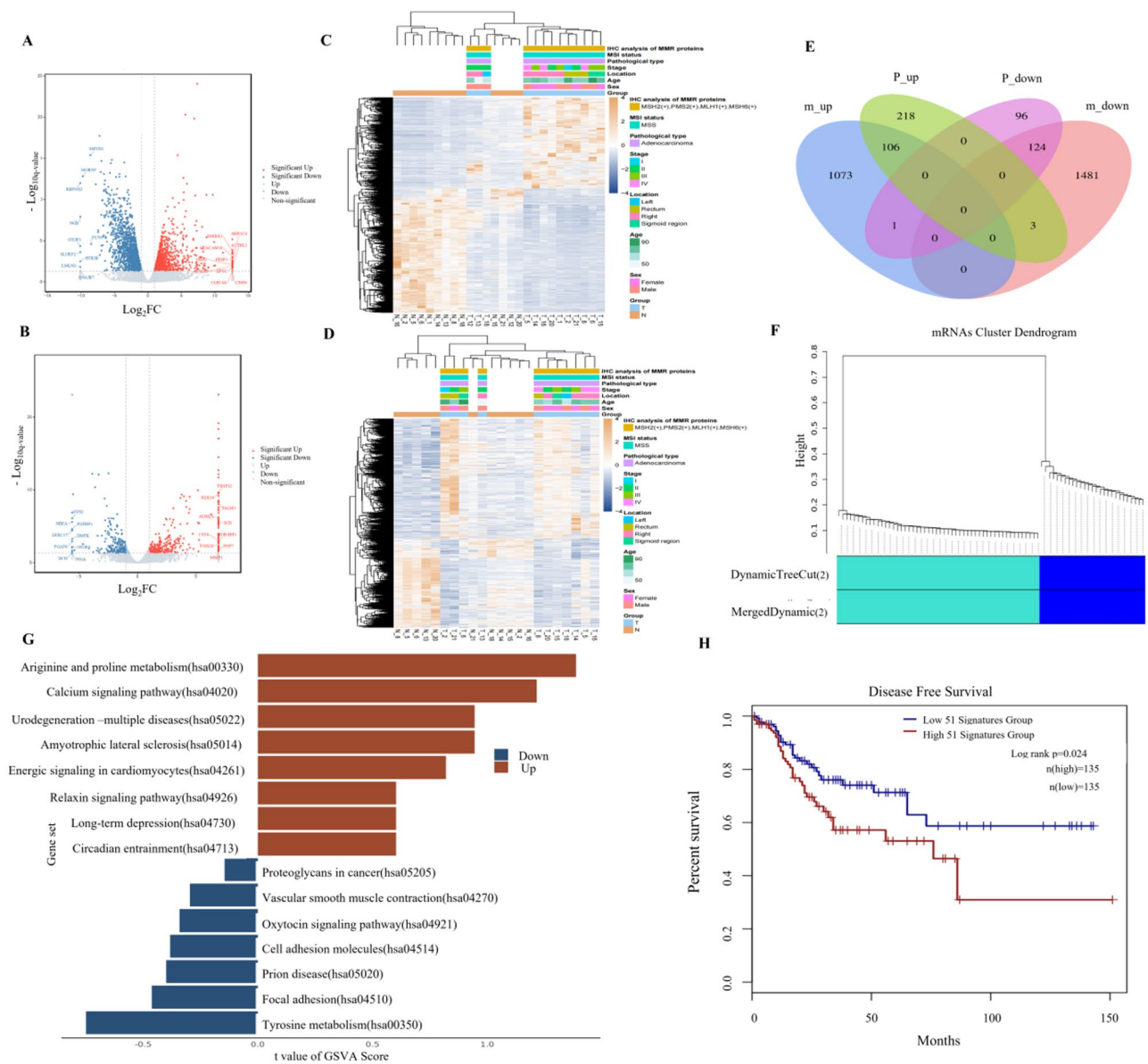


Fig. 1 Identification of hub genes using WGCNA and validation against external databases. **(A)** Volcano plot of mRNA expression in 13 CRC tissues and paired NATs. **(B)** Volcano plot of protein expression in 11 CRC tissues and paired NATs. **(C)** Hierarchical heatmap of DEGs in 13 CRC tissues and paired NATs. **(D)** Hierarchical heatmap of DEPs in 11 CRC tissues and paired NATs. **(E)** Venn diagram illustrating the overlap between mRNAs and proteins with consistent expression patterns. **(F)** WGCNA co-expression module analysis of mRNAs. **(G)** GSEA of 52 hub genes in the turquoise module. **(H)** Survival analysis of the gene set in the turquoise module. Abbreviations: DEGs, differentially expressed genes; DEPs, differentially expressed proteins; WGCNA, weighted gene co-expression network analysis; GSEA, gene set enrichment analysis

protein expression, 27 upregulated and 52 downregulated genes with $|\log_2 \text{FC}| > 2$ were selected for further analysis. These 79 genes formed two co-expression modules based on WGCNA analysis: M1 (52 genes highlighted in turquoise) and M2 (27 genes labeled in blue for mRNAs and gray for proteins) (Fig. 1F and Supplementary Fig. S2A) [22]. Pearson correlation analysis was performed to assess the relationship between mRNA and protein module eigengenes and traits, selecting significant associations with a correlation coefficient ≥ 0.3 and p -value < 0.05 , with mRNA and protein modules selected separately (see Supplementary Fig. S2B and S2C). The M1 module, which showed strong co-expression at both mRNA and protein levels (Supplementary Fig. S2D, and S2E), was found to be associated with tumor cell proliferation, metastasis, amino acid metabolism, and signal transduction, as determined by Gene Set Variation Analysis (GSVA) [26] (Fig. 1G). Further analysis using the GEPIA2 [27] and CPTAC2 [28] databases confirmed the decreased RNA and protein expression in CRC tissue compared to normal colon tissue for 42 genes in the M1 module (Supplementary Fig. S2F). Additionally, survival analysis of Disease-Free Survival (RFS) using the GEPIA2 database showed that altered mRNA expression levels of 51 genes in the M1 module were associated with poor prognosis in CRC patients, with 50% high and 50% low expression as cutoff values for grouping (Fig. 1H).

We further explored the role of lncRNAs in regulating the mRNA/protein co-expression module (M1). Of the 1,394 DELncs, 436 showed $|\log_2 \text{FC}| > 5$ (Supplementary Fig. S3A). Then, we examined the co-expression correlation between 436 lncRNAs and the 52 mRNA/protein expressions in the M1 module (Supplementary Fig. S3B and S3C). Correlation analysis between these lncRNAs and the 52 mRNA/protein expressions in the M1 module revealed a significant association for 174 lncRNAs ($P < 0.05$) (Fig. 2A). Among them, 22 candidate lncRNAs, including 2 known and 20 novel lncRNAs, were identified as potential regulators based on a correlation threshold ($r > 0.9$) between lncRNA and mRNA [29], as well as a significant correlation with protein expression (Fig. 2B).

To better understand the metabolic changes in CRC, we performed metabolomic profiling on 11 CRC tissues and matched NATs, each with three replicates. PLS-DA analysis revealed that metabolic features could effectively distinguish CRC tissues from NATs (Fig. 2C), with good predictive ability ($R^2 = 0.685$, $Q^2 = 0.508$) (Fig. 2D) [30]. We identified 91 DEMs ($P < 0.05$ and $|\log_2 \text{FC}| > 0$) (Supplementary Fig. S3D), which were enriched in pathways related to amino acid metabolism, according to functional analysis using MetaboAnalyst (Supplementary Fig. S3E) [31]. Through ROC analysis, we found 30 DEMs with AUC values > 0.7 ; among these, ATRA and 13,14-dihydro-15-keto-PGE2 were significantly reduced

in CRC tissues compared to NATs (AUC = 0.832 and 0.818, respectively) (Fig. 2E). Using the STAMP approach [32], we identified and selected the top 30 DEMs (Supplementary Fig. S3F), and then explored the correlation between these two sets of DEMs and gene or protein expression in the M1 module (Supplementary Fig. S3G and H). Our findings revealed that 17 DEMs were significantly correlated with 40 genes in the M1 module both at mRNA and protein levels, 15 of which were among the top 30 DEMs identified by both STAMP and ROC analysis (Fig. 2F). Furthermore, we identified 10 metabolites from 15 candidate markers that showed significant correlations with 29 molecular entities at both the mRNA and protein levels, suggesting their potential as reliable biomarkers for CRC.

Taken together, by linking lncRNAs to metabolites through mRNA and protein interactions, we uncovered a complex interaction network involving 22 lncRNAs, 14 mRNAs/proteins, and 9 metabolites (Fig. 2G).

In vitro validation of multi-level molecular expression

To validate the associations among lncRNAs, mRNAs/proteins, and metabolites, we focused on a specific network branch involving a novel lncRNA 60967.1, its potential target genes, and related metabolites (Fig. 2G). This lncRNA exhibited significant associations with 12 out of 14 genes and 6 out of 9 metabolites within the network, suggesting its potential roles in CRC. Sequencing data revealed that lncRNA 60967.1 is 370 bp in length and located on chromosome 14 (Supplementary Table S4). We evaluated its expression by qRT-PCR in three CRC cell lines, a human colon mucosal epithelial cell line (NCM460), and tumor and adjacent normal tissues from 12 additional CRC patients (Supplementary Table S5). Notably, the expression of lncRNA 60967.1 was significantly downregulated in CRC cell lines compared to the normal control (Fig. 3A). This finding was further corroborated by qRT-PCR analysis of the 12 CRC tissue samples and matched NATs (Fig. 3B).

We then performed qRT-PCR analysis of the mRNA levels of lncRNA-targeted genes and identified that the mRNA levels of three target genes, CAP2, GNAO1, and PLCD4, were significantly decreased in the three CRC cell lines (DLD1, HCT8, SW480) compared to NCM460 (Fig. 3C, Supplementary Fig. S4A and S4B), as well as in 12 CRC tissues relative to matched NATs (Fig. 3D, Supplementary Fig. S4C and S4D). Next, we examined the protein expression of CAP2, GNAO1, and PLCD4 in both cultured CRC cells and tissue samples using Western blotting. Among the three, only PLCD4 consistently showed a significant reduction in protein levels in both CRC cells and tissue samples (Fig. 3E and F). Immunohistochemistry (IHC) analysis further confirmed the

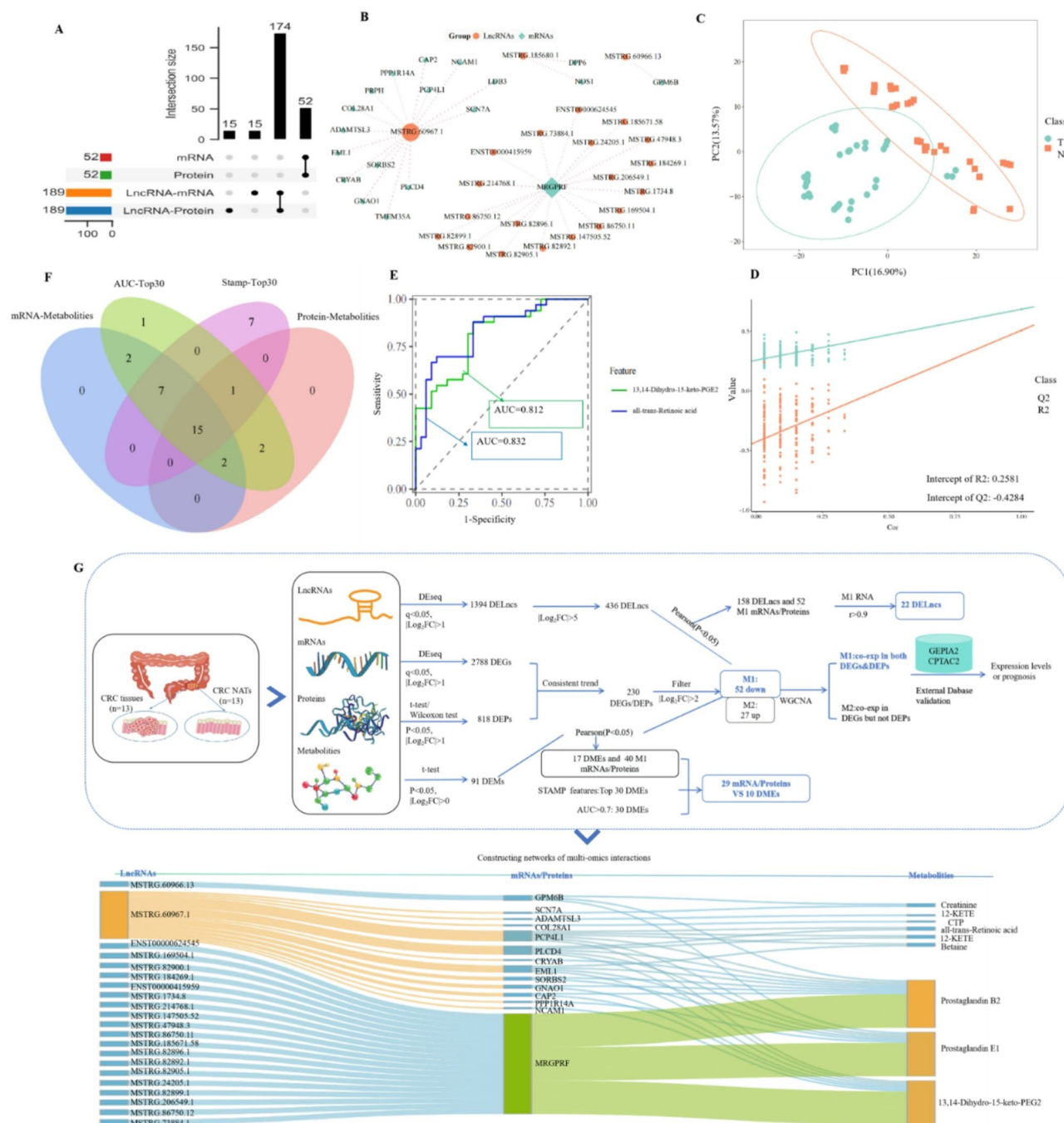


Fig. 2 Integrated multi-omics analysis reveals network associations among lncRNAs, mRNAs, proteins, and metabolites. **(A)** Upset plot of lncRNAs showing statistically significant associations with mRNAs and proteins. **(B)** Network diagram depicting lncRNA interactions with target genes. **(C)** PLS-DA analysis of metabolomic data. **(D)** Evaluation of the PLS-DA model for metabolomic data, including model performance metrics and the separation of sample groups. **(E)** ROC analysis identifying two metabolites with AUC > 0.8. **(F)** Venn diagram illustrating the overlap among mRNA–metabolite pairs, protein–metabolite pairs, the top 30 AUC metabolites, and the top 30 STAMP metabolites. **(G)** Bioinformatic analysis reveals predicted associations among lncRNAs, mRNAs/proteins, and metabolites. Top: data analysis pipeline; Bottom: network of lncRNAs, mRNAs/proteins, and metabolites. Abbreviations: ROC, receiver operating characteristic; AUC, area under the curve; PLS-DA, partial least squares discriminant analysis; STAMP, statistical analysis of taxonomic and functional profiles

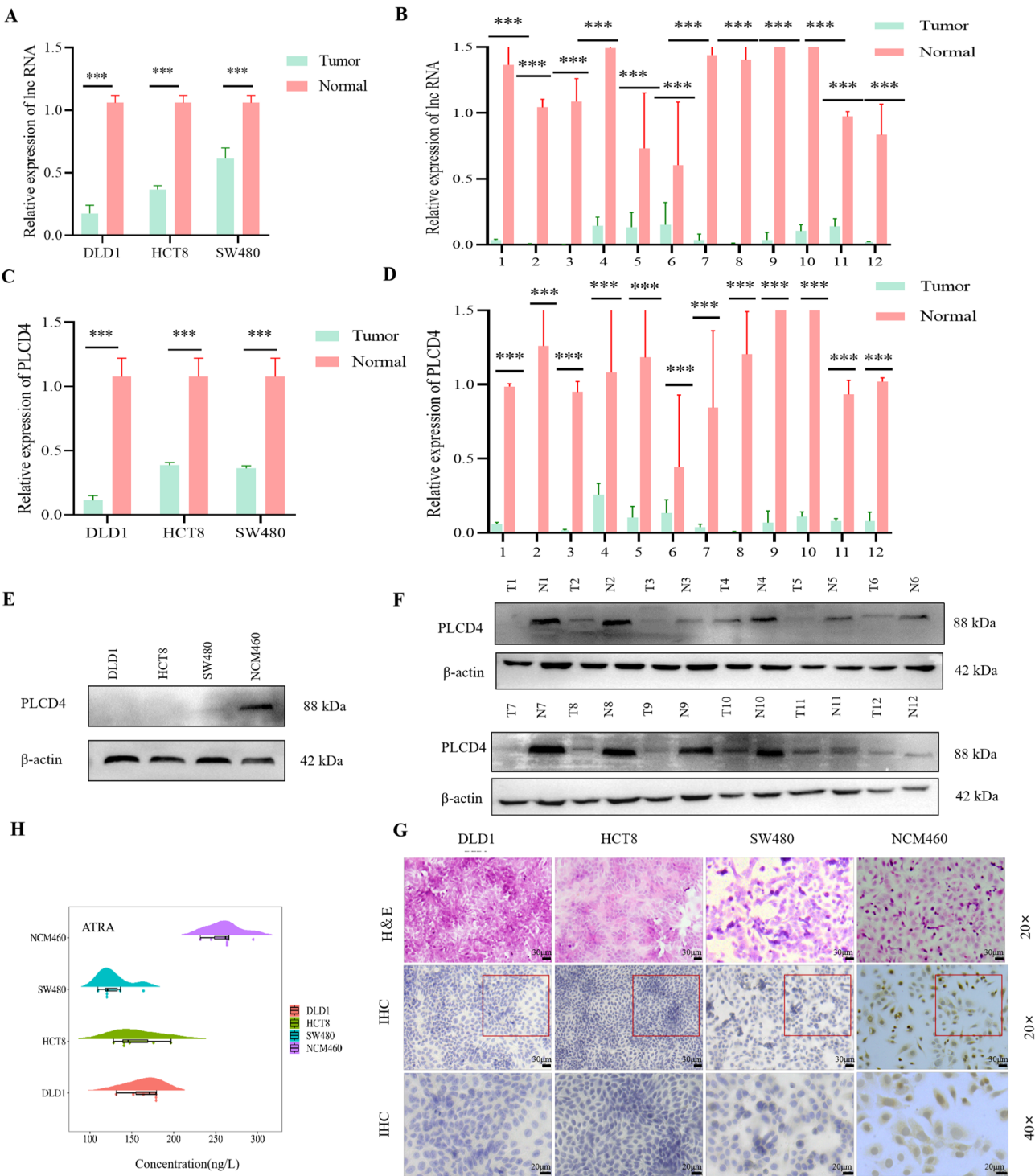


Fig. 3 Experimental validation of mRNA, lncRNA, and metabolite levels. **(A)** Expression of lncRNA 60967.1 in CRC cell lines (DLD1, HCT8, SW480) relative to the normal colon cell line (NCM460), measured by qRT-PCR. **(B)** qRT-PCR validation of lncRNA 60967.1 expression in 12 paired CRC tumor and normal tissues. **(C)** qRT-PCR analysis of PLCD4 mRNA levels in the three CRC cell lines (DLD1, HCT8, SW480) and the normal colon cell line. **(D)** qRT-PCR validation of PLCD4 mRNA levels in 12 paired CRC tumor and normal tissues. **(E-F)** Western blot analysis of PLCD4 protein expression in the three CRC cell lines (DLD1, HCT8, SW480) and the normal colon cell line (NCM460) **(E)** and 12 paired tumor (T#) and normal (N#) tissues **(F)**. **(G)** IHC analysis of PLCD4 protein expression in the three CRC cell lines (DLD1, HCT8, SW480) and the normal colon cell line (NCM460). **(H)** ELISA-based quantification of ATRA levels in culture supernatants from the three CRC cell lines (DLD1, HCT8, SW480) and the normal colon cell line (NCM460). *** $P < 0.01$ (t test)

decreased expression of PLCD4 protein in CRC tumor cells (Fig. 3G).

Notably, PLCD4, a member of the phosphatidylinositol-specific phospholipase C (PLC) family, hydrolyzes phosphatidylinositol-4,5-bisphosphate (PIP₂) into inositol 1,4,5-trisphosphate (IP₃), a second messenger that triggers calcium (Ca²⁺) mobilization, and diacylglycerol, which activates protein kinase C (PKC), a key component in signaling pathways [33–35]. We then performed a pathway analysis of PLCD4 using the KEGG database (<https://www.kegg.jp>). To evaluate the levels of PIP₂, IP₃, and PKC, we performed IHC assays on CRC cell lines and the normal intestinal epithelial cell line NCM460. The expression levels of PIP₂ and its hydrolyzed product, IP₃, were not significantly downregulated in the CRC cell lines compared to the control. Similarly, no significant differences in PKC protein levels were observed between the CRC cell lines and the control cells. These results suggest that PLCD4 may exert its function through alternative signaling pathways (Supplementary Fig. S5A and S5B).

Previous studies have reported significant downregulation of ATRA synthesis enzymes in CRC, suggesting reduced ATRA levels in CRC tumors [36, 37]. To explore this, we assessed the levels of the metabolite ATRA in the cell-free supernatant of cultured CRC cell lines and NCM460 cells using an ELISA assay. Consistent with previous findings, we observed a significant reduction in ATRA levels in the CRC cell lines compared to normal control cells (Fig. 3H).

Overall, our cellular and tissue-based validation experiments revealed a critical regulatory axis comprising lncRNA 60967.1, PLCD4, and the metabolite ATRA. These findings reinforce the reliability of the identified network and suggest a potential role for these biomolecules in CRC pathogenesis.

lncRNA 60967.1 modulates the PLCD4/ATRA axis and reverses IFN- γ resistance in CRC cells

To investigate the regulatory role of lncRNA 60967.1 on the PLCD4/ATRA axis, we first examined its physical localization relative to PLCD4 mRNA using fluorescence in situ hybridization (FISH). As shown in Fig. 4A, lncRNA 60967.1 and PLCD4 mRNA were colocalized in the cytoplasm. Next, we evaluated whether lncRNA 60967.1 interacts with PLCD4 protein by performing an RIP assay in NCM460 cells, followed by qRT-PCR and Western blot analysis. The results demonstrated that lncRNA 60967.1 binds to PLCD4 protein significantly more than to the IgG control (Fig. 4B), and Western blotting confirmed the enrichment of PLCD4 in the immunoprecipitated complex (Fig. 4C). These findings suggest a direct interaction between lncRNA 60967.1 and PLCD4. Subsequently, we performed lentiviral expression of lncRNA 60967.1

in CRC cells. Overexpression of lncRNA 60967.1 led to increased levels of PLCD4 at both the mRNA (Fig. 4D) and protein (Fig. 4E) levels, as well as elevated concentrations of the metabolite ATRA (Fig. 4F).

ATRA is a well-established metabolite that regulates key cellular processes, including cell growth, differentiation, and apoptosis and modulates immune responses [38–40]. However, our in vitro functional assays showed that overexpression of lncRNA 60967.1, and the resulting increase in ATRA levels, did not significantly affect CRC cell proliferation or apoptosis (data not shown). Given that DLD1 and SW480 cell lines are known to be resistant to IFN- γ , a critical cytokine involved in activating immune responses [41], and that synergistic effects of ATRA and IFN- γ have been reported in animal models and cultured cells [42–44], we investigated whether the lncRNA 60967.1-regulated PLCD4/ATRA axis could modulate IFN- γ resistance in CRC cells. Notably, overexpression of lncRNA 60967.1 significantly reduced CRC cell proliferation in response to IFN- γ stimulation (Fig. 4G–I) and increased IFN- γ -induced apoptosis (Supplementary Fig. S6A–F). While CRC cells transfected with control lentivirus only had no significant impact on IFN- γ stimulation (Supplementary Fig. S6G).

We next investigated the expression levels of the IFN- γ receptor subunits, IFNGR1 and IFNGR2. Overexpression of lncRNA 60967.1 in CRC cells resulted in a significant increase in IFNGR1 mRNA levels. In contrast, IFNGR2 mRNA expression showed variability across the three CRC cell lines tested (Fig. 4J). This upregulation of IFNGR1 was further confirmed at the protein level (Fig. 4K). To explore the potential difference in IFNGR1 expression between CRC and normal cells, we compared IFNGR1 expression in CRC cells and NCM460 cells. The results indicated that IFNGR1 expression was significantly lower in CRC cells compared to NCM460 cells (Supplementary Fig. S6H–I). Additionally, we observed that ATRA stimulation in CRC cells induced the upregulation of IFNGR1 expression, although IFNGR2 mRNA expression remained variable across the different CRC cell lines (Fig. 4L).

These findings suggest that lncRNA 60967.1 regulates the PLCD4/ATRA axis in CRC cells and contributes to the partial reversal of IFN- γ resistance by upregulating the IFN- γ receptor subunit IFNGR1, thereby enhancing the response to immune stimulation.

PLCD4 acts as a tumor suppressor in CRC by inhibiting migration, invasion, and tumor growth

PLCD4 is a critical component of the lncRNA/PLCD4/ATRA axis. To investigate its role in CRC development, we generated a PLCD4 overexpression vector and transfected it into two CRC cell lines, DLD1 and HCT116. In vitro migration and invasion assays revealed that PLCD4

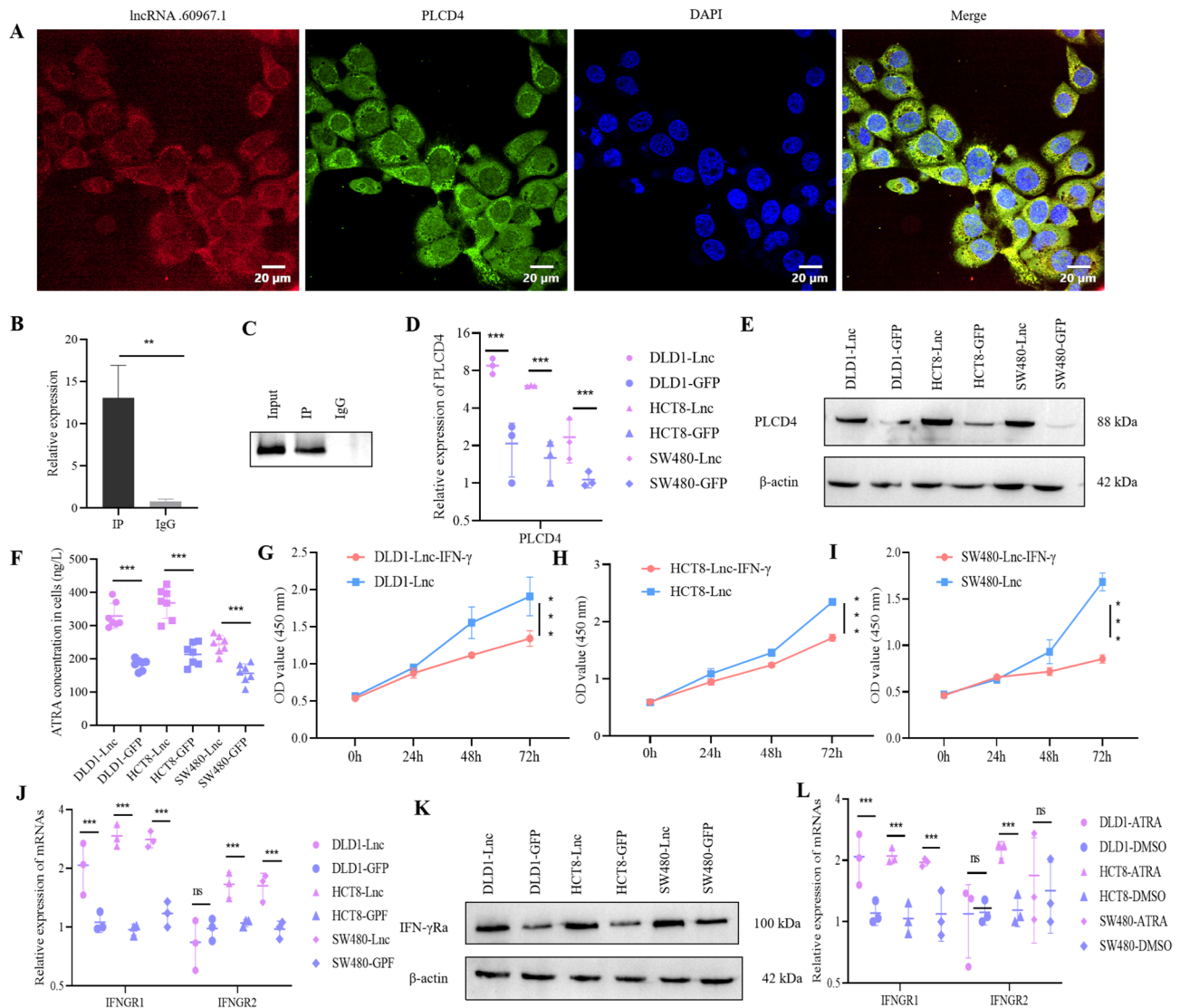


Fig. 4 Molecular and functional effects of lncRNA 60967.1 on PLCD4 expression, ATRA levels, and CRC cell proliferation. **(A)** Fluorescence in situ hybridization (FISH) showing the localization of lncRNA 60967.1 and PLCD4 mRNA in NCM460 cells. **(B)** RIP assay followed by qRT-PCR analysis of lncRNA 60967.1 in immunoprecipitated (IP) and IgG control groups. **(C)** RIP assay followed by Western blot analysis of PLCD4 in the input, immunoprecipitated (IP), and IgG control groups. **(D)** qRT-PCR analysis of PLCD4 mRNA in CRC cells (DLD1, HCT8, SW480) transfected with GFP control or lncRNA 60967.1 vector. **(E)** Western blot analysis of PLCD4 protein expression in CRC cells (DLD1, HCT8, SW480) with GFP or lncRNA 60967.1 vector. **(F)** ELISA measurement of ATRA levels in CRC cells (DLD1, HCT8, SW480) with GFP or lncRNA 60967.1 vector. **(G-I)** CCK-8 assay for CRC cell proliferation (DLD1, HCT8, SW480) transfected with lncRNA 60967.1 vector, followed by IFN-γ stimulation. **(J)** qRT-PCR analysis of IFNGR1/IFNGR2 mRNA in CRC cells transfected with GFP or lncRNA 60967.1 vector. **(K)** Western blot analysis of IFN-γRa protein in CRC cells (DLD1, HCT8, and SW480) transfected with GFP or lncRNA 60967.1 vector. **(L)** qRT-PCR evaluation of IFNGR1/IFNGR2 mRNA in CRC cells (DLD1, HCT8, and SW480) stimulated by ATRA or DMSO. Abbreviation: CCK-8, Cell Counting Kit-8. NS: not significant (t-test); **P < 0.05, ***P < 0.01 (t-test)

overexpression significantly inhibited the invasive and migratory capacities of CRC cells compared with cells transfected with the empty vector control, suggesting that PLCD4 reduces cell motility and may impede tumor progression (Fig. 5A). Furthermore, HCT116 cells overexpressing PLCD4 were injected into Balb/c nude mice. Analysis of tumor volume and weight showed a significant reduction in the PLCD4 overexpression group

compared to the vector control group, confirming the tumor suppressive effect of PLCD4 (Fig. 5B and C, and 5D).

Conversely, two distinct siRNAs were used to knock down PLCD4 in three CRC cell lines. Western blot analysis confirmed a significant reduction in PLCD4 expression in all three cell lines (Fig. 5E). Notably, migration and invasion assays showed that, compared to cells transfected with the empty vector control, PLCD4 knockdown

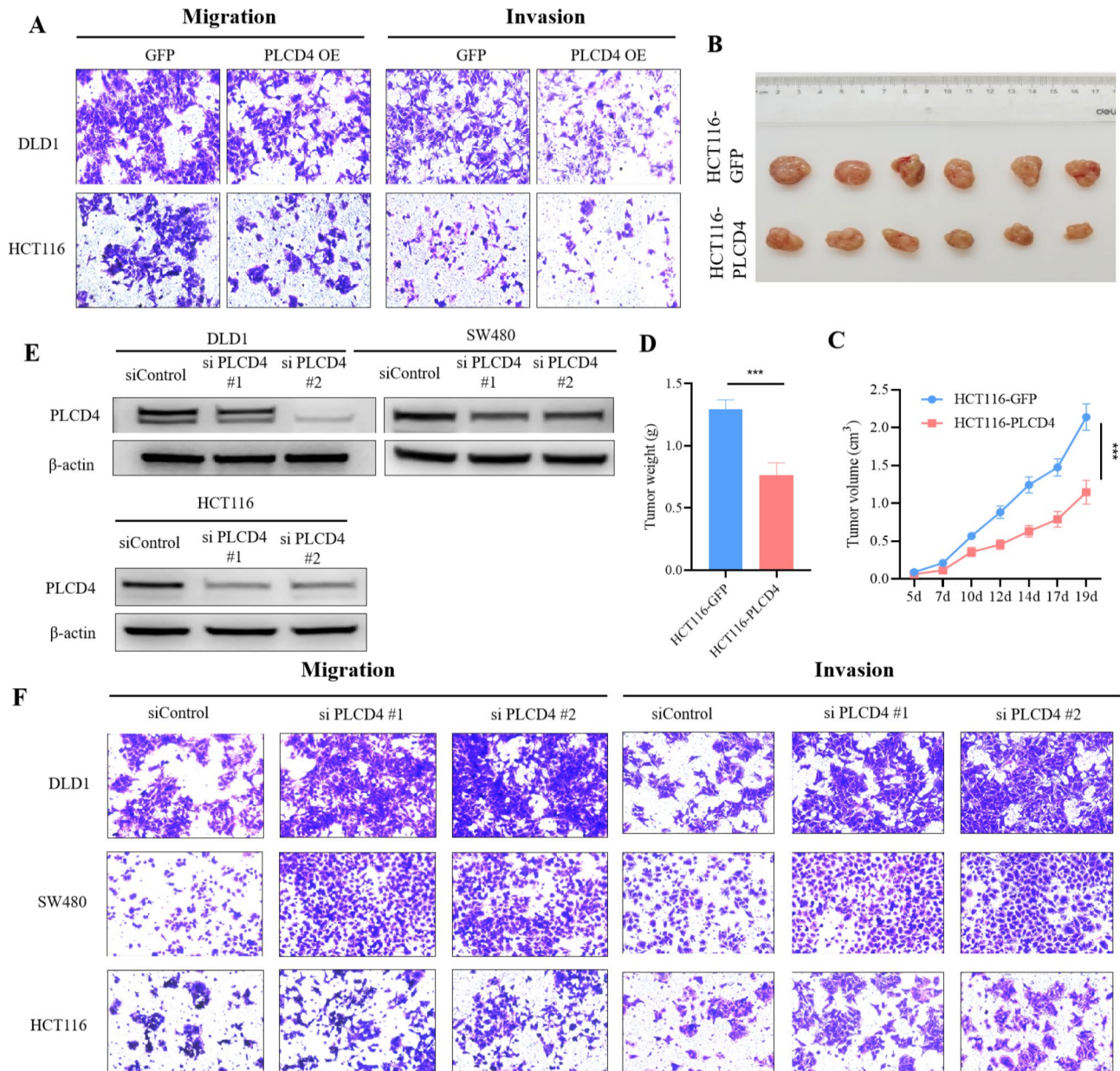


Fig. 5 PLCD4 acts as a tumor suppressor in CRC. **(A)** Migration and invasion assays using two CRC cell lines (HCT116 and DLD1) transfected with either GFP (NC) or PLCD4 expression (PLCD4 OE) vectors. **(B)** Tumors from Balb/c nude mice injected with HCT116 cells transduced with either GFP (Top) or PLCD4 (Bottom) expression vectors. **(C)** Tumor growth over time in Balb/c nude mice injected with HCT116 cells transduced with GFP (blue) or PLCD4 (pink) expression vectors. **(D)** Measurement of tumor weight in Balb/c nude mice injected with HCT116 cells transduced with GFP (blue) or PLCD4 (pink) expression vectors. **(E)** Western blot analysis of PLCD4 expression in CRC cell lines (DLD1, SW480, HCT116) following siRNA-mediated knockdown (siPLCD4#1 or siPLCD4#2) or non-targeting control siRNA (siControl). **(F)** Migration and invasion assays using CRC cell lines (DLD1, SW480, HCT116) transfected with two PLCD4-targeting siRNAs (siPLCD4#1 or siPLCD4#2) or non-targeting control siRNA (siControl)

significantly enhanced the migratory and invasive potential of CRC cells (Figs. 5F).

Lastly, we calculated the immune score, stromal score, and tumor purity for 650 TCGA-CRC samples using the ESTIMATE algorithm, which allowed us to gain insights into the infiltration patterns within the CRC TME. Pearson's correlation analysis revealed a significant positive correlation between PLCD4 mRNA expression and both

the ImmuneScore and StromalScore, indicating enhanced infiltration of immune and stromal cells within the TME. In contrast, a negative correlation was observed between PLCD4 expression and Tumor Purity, suggesting a reduction in tumor cell content as immune and stromal components increase (Supplementary Fig. S7B). To validate these results, a similar analysis was conducted using the xCell algorithm, which corroborated the findings from

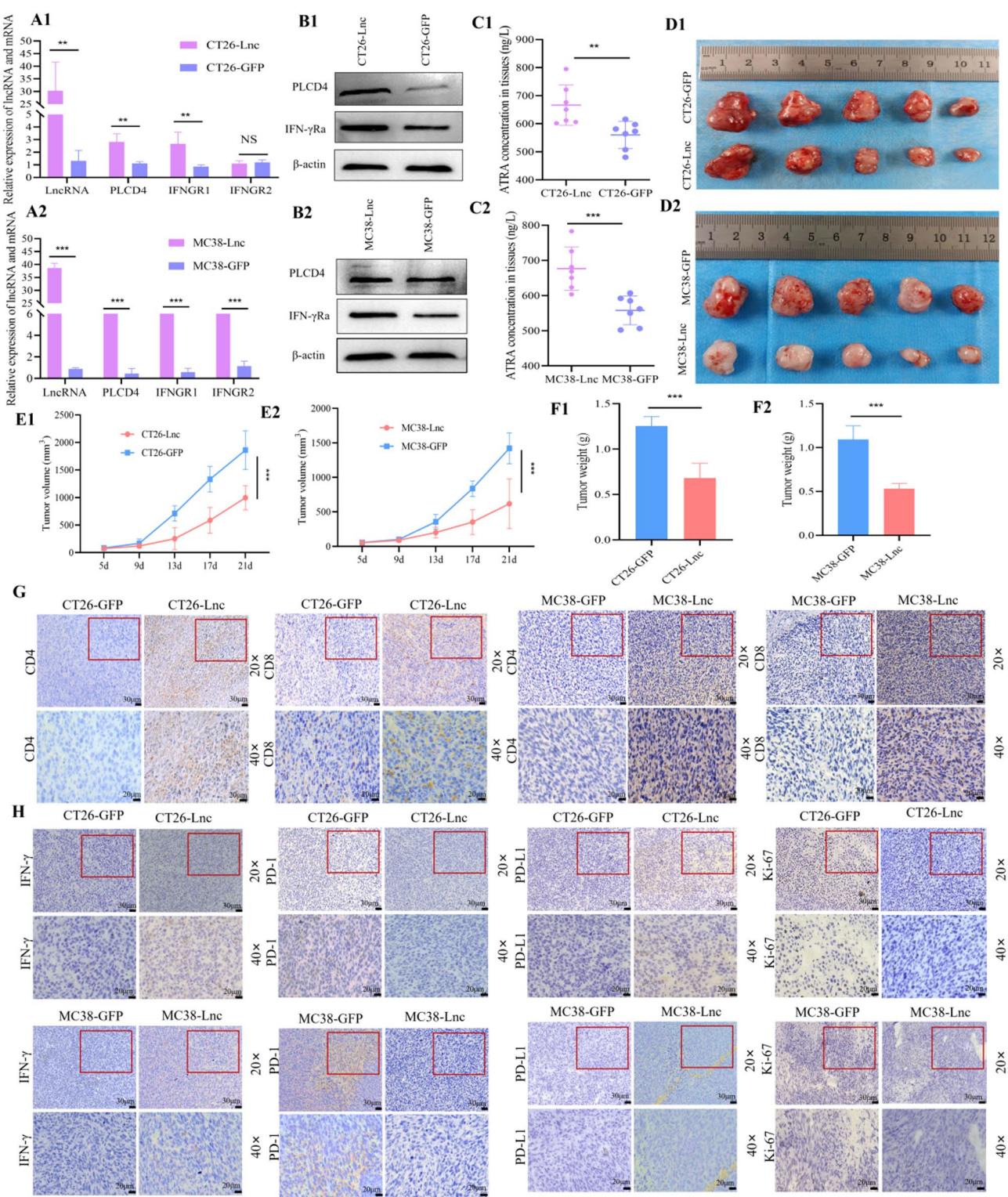


Fig. 6 (See legend on next page.)

the ESTIMATE algorithm (Supplementary Fig. S7C). These findings suggest that PLCD4 may play a crucial role in modulating the TME by promoting the infiltration of stromal and immune cells, potentially influencing disease progression and therapeutic outcomes.

(See figure on previous page.)

Fig. 6 lncRNA 60967.1 overexpression promotes PLCD4 and ATRA expression, enhances immune cell infiltration, and reduces tumor growth in mouse CRC models. **(A1–A2)** qRT-PCR analysis of lncRNA 60967.1, PLCD4, and IFNGR1/2 expression in tumor tissues from mice injected with mouse CRC cells (CT26, **A1**; MC38, **A2**) transfected with lncRNA 60967.1 or GFP vectors. **(B1–B2)** Western blot analysis of PLCD4 and IFN- γ R α proteins in tumor tissues from mice injected with CT26 cells (**B1**) or MC38 cells (**B2**) transfected with lncRNA 60967.1 or GFP vectors. **(C1–C2)** ELISA analysis of ATRA in tumor tissues from mice injected with CT26 cells (**C1**) or MC38 cells (**C2**) transfected with lncRNA 60967.1 or GFP vectors. **(D1–D2)** Tumors harvested from Balb/c mice that were subcutaneously injected with either CT26 cells (**D1**) or MC38 cells (**D2**). Each cell line was transfected with GFP or lncRNA 60967.1 vectors prior to injection, allowing comparison of tumor growth and size between the control and experimental groups. **(E1–E2)** Tumor growth curves in Balb/c mice injected with CT26 cells (**E1**) or MC38 cells (**E2**) transfected with either GFP or lncRNA 60967.1 vectors. Tumor sizes were measured at regular intervals to compare progression between the control (GFP) and lncRNA 60967.1 overexpression groups. **(F1–F2)** Measurement of tumor weight in Balb/c nude mice injected with CT26 cells (**F1**) or MC38 cells (**F2**), transfected with either GFP or lncRNA 60967.1 expression vectors. **(G)** IHC analysis of CD4 and CD8 expression in tumor tissues from Balb/c mice subcutaneously injected with either CT26 or MC38 cells. Each cell line was transfected with GFP or lncRNA 60967.1 vectors before injection, enabling a comparison of immune cell infiltration between control and lncRNA 60967.1-overexpressing groups. **(H)** IHC analysis of IFN- γ , PD-1, PD-L1, and Ki67 expression in tumor tissues from Balb/c mice subcutaneously injected with either CT26 or MC38 cells. Each cell line was transfected with GFP or lncRNA 60967.1 vectors before injection, allowing for a comparison of the functional states or activation/exhaustion profiles of immune cells between the control and lncRNA 60967.1-overexpressing groups. NS indicates no significant difference (t-test); ** $P < 0.05$, *** $P < 0.01$ (t-test)

Taken together, these findings demonstrate that PLCD4 acts as a tumor suppressor in CRC by inhibiting cell motility and tumor growth.

lncRNA 60967.1 suppresses tumor development by modulating the tumor microenvironment via PLCD4 /ATRA regulation

To assess the impact of lncRNA 60967.1 overexpression on the tumor microenvironment, we transplanted CT26 and MC38 murine CRC cells—transfected with either an lncRNA 60967.1 expression vector or a control vector—into immunocompetent BALB/c or C57BL/6 mice. Overexpression of lncRNA 60967.1 led to a significant increase in both PLCD4 and IFNGR1 expression at the mRNA and protein levels in the mouse tumor tissues (Fig. 6A1, 6A2, 6B1 and 6B2). In parallel, lncRNA 60967.1 overexpression also resulted in elevated ATRA levels (Fig. 6C1 and 6C2). In addition, mice bearing tumors derived from cells overexpressing lncRNA 60967.1 exhibited significant reductions in tumor volume (Fig. 6D1 and 6D2), proliferation rate (Fig. 6E1 and 6E2), and tumor weight (Fig. 6F1 and 6F2) compared to control groups.

To further investigate the impact on immune cell infiltration, IHC was performed to evaluate CD4⁺ and CD8⁺ cell populations in the tumor tissues. As expected, a significant increase in both CD4⁺ and CD8⁺ T cells (Fig. 6G) was observed in the CT26-Lnc group compared to the CT26-GFP group, suggesting that lncRNA 60967.1 promotes immune infiltration within the tumor microenvironment. Furthermore, we performed additional characterization of immune cell activation, exhaustion, and proliferation in the tumor microenvironment using IHC assays. Specifically, we analyzed the effects of lncRNA 60967.1 on the following markers: activation markers (IFN- γ and Granzyme B), exhaustion markers (PD-1 and TIM-3), and proliferation marker (Ki67) in CT26 and MC38 mouse tumor tissues. Our results showed that overexpression of lncRNA 60967.1 significantly increased IFN- γ expression in the tumor microenvironment, suggesting enhanced immune activation, as

shown in Fig. 6H. In contrast, PD-1 and Ki67 levels were significantly reduced, suggesting a potential suppression of immune exhaustion and decreased cell proliferation (Fig. 6H). However, we did not observe statistically significant changes in Granzyme B and TIM-3 expression, suggesting that the effects of lncRNA 60967.1 may be more selective in its modulation of immune cell activation. These findings indicate that lncRNA 60967.1 overexpression enhances key immune and signaling components, ultimately suppressing tumor growth and promoting a more active immune response *in vivo*.

Overexpression of lncRNA enhances the efficacy of anti-PD-1 therapy in a murine CRC model

lncRNAs have emerged as key regulators of immune evasion and therapeutic resistance in CRC [45]. Building on the observed tumor-suppressive and immune-modulatory effects of lncRNA 60967.1 in the tumor microenvironment, we next explored whether its overexpression could enhance the efficacy of immune checkpoint blockades in a murine CRC model. Overexpression of lncRNA 60967.1 via lentiviral transduction led to a significant upregulation of the immune-related checkpoint molecule PD-L1, while the expression patterns of CD47 and CD276 were inconsistent across three CRC cell lines, as measured by qRT-PCR (Fig. 7A1, 7A2 and 7A3). Western blot analysis confirmed that the observed changes in PD-L1 were consistent at protein levels across three CRC cell lines (Fig. 7B).

To further dissect the functional importance of lncRNA 60967.1, we used three different siRNAs in HCT8 cells, ultimately selecting siRNA-1 for its higher specificity (Fig. 7C). Knockdown of lncRNA 60967.1 resulted in reduced expression of PLCD4, IFNGR1, and PD-L1 at both the mRNA and protein levels (Fig. 7D–E). These observations suggest that lncRNA 60967.1 may play a regulatory role in immune checkpoint pathways, potentially affecting tumor immune evasion mechanisms.

Based on these findings, we hypothesized that lncRNA 60967.1 overexpression could synergize with

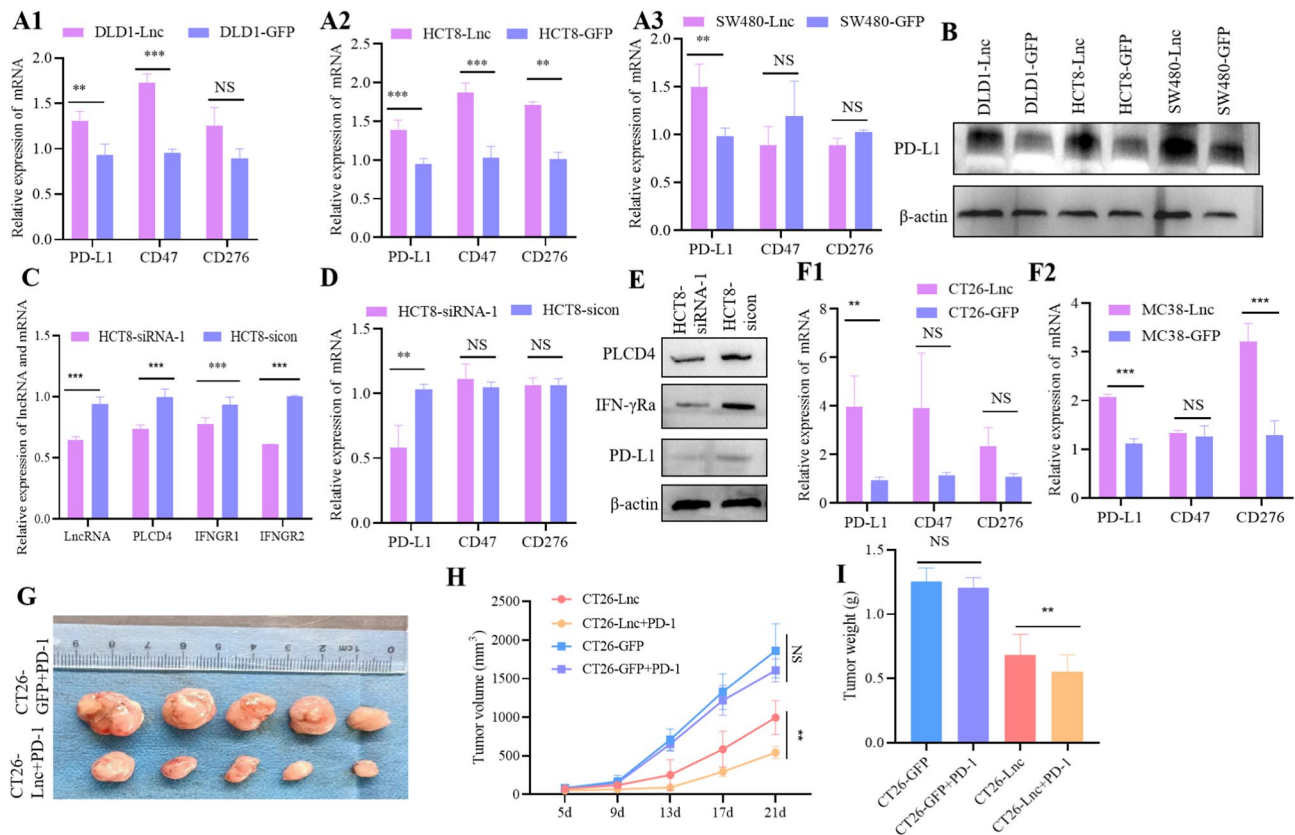


Fig. 7 LncRNA 60967.1 upregulates immune checkpoint gene expression and enhances anti-PD-1 efficacy in CRC mouse models. (**A1-A3**) qRT-PCR analysis of PD-L1, CD47, and CD276 mRNA levels in three CRC cell lines (DLD1, **A1**; HCT8, **A2**; and SW480, **A3**) transfected with either a GFP control or an LncRNA 60967.1 expression vector. (**B**) Western blot analysis of PD-L1 levels in DLD1, HCT8, and SW480 cells transfected with either a GFP control or a LncRNA 60967.1 expression vector. (**C**) qRT-PCR analysis of LncRNA 60967.1, PLCD4, IFNGR1, and IFNGR2 expression in HCT8 cells transfected with an siRNA vector targeting LncRNA 60967.1 (HCT8-siRNA-1) or a non-targeting control vector (HCT8-NC). (**D**) qRT-PCR validation of PD-L1, CD47, and CD276 mRNA expression in HCT8 cells transfected with siRNA targeting LncRNA 60967.1 (HCT8-siRNA-1) or a non-targeting control (HCT8-NC). (**E**) Western blot analysis of PD-L1 expression in HCT8 cells transfected with siRNA targeting LncRNA 60967.1 (HCT8-siRNA-1) or a non-targeting control (HCT8-NC). (**F1-F2**) qRT-PCR measurement of immune checkpoint gene mRNA levels (PD-L1, CD47, and CD276) in tumor tissues from Balb/c mice injected with CT26 cells (**F1**) or MC38 cells (**F2**). Cell lines were transfected with GFP (control) or LncRNA 60967.1 vectors before injection to compare checkpoint gene expression. (**G**) Tumors harvested from Balb/c mice that were subcutaneously injected with CT26 cells transfected with either GFP (Top) or LncRNA 60967.1 vectors (Bottom), followed by intraperitoneal administration of anti-PD-1 monoclonal antibody. (**H**) Tumor growth over time in Balb/c nude mice injected with CT26 cells transfected with either GFP or LncRNA 60967.1 vectors, followed by intraperitoneal administration of anti-PD-1 monoclonal antibody. (**I**) Tumor weight in Balb/c nude mice injected with CT26 cells transfected with either GFP or LncRNA 60967.1 vectors, followed by intraperitoneal administration of anti-PD-1 monoclonal antibody. NS indicates no significant difference (t-test); ** $P < 0.05$, *** $P < 0.01$ (t-test)

immunotherapy. To test this hypothesis, we first examined whether overexpression of LncRNA 60967.1 increases PD-L1 levels in the murine CRC cell lines CT26 and MC38. qPCR analysis confirmed that PD-L1 expression was elevated in these cell lines following LncRNA 60967.1 overexpression (Fig. 7F1 and 7F2). Next, we established a murine CRC model by transplanting CT26 cells engineered to overexpress LncRNA 60967.1 into immunocompetent mice. When treated with anti-PD-1 monoclonal antibody (clone RMP1-14), the LncRNA overexpression group exhibited a significantly enhanced anti-tumor response with significant reductions in tumor volume (Fig. 7G), tumor weight (Fig. 7H), and proliferation rate (Fig. 7I), outperforming the LncRNA overexpression group alone. These data support the notion that

combining LncRNA-targeted therapy with PD-1 blockade could offer a more effective therapeutic approach to CRC.

Together, these results indicate that LncRNA 60967.1 may suppress CRC cell proliferation by modulating the tumor microenvironment and regulating key immune checkpoints. While additional investigations are needed, our findings point toward a similar inhibitory effect of LncRNA 60967.1 on human CRC cells through its capacity to influence immune-related pathways, highlighting its potential as a combinatorial target for immunotherapy.

Discussion

Multi-omics analysis has become a powerful tool for uncovering pathogenic mechanisms in human diseases, particularly in cancer [46, 47]. In this study, we integrated transcriptomic, proteomic, and metabolomic data of CRC tissues and matched NATs collected from 13 patients. The analysis revealed a complex interaction network involving 22 lncRNAs, 14 mRNAs/proteins, and 9 metabolites (Fig. 2G). Among these, lncRNA 60967.1 emerged as a key regulator. Validation in CRC cell lines and an additional patient cohort confirmed the significant downregulation of both lncRNA 60967.1 and PLCD4. Furthermore, a concurrent reduction in the metabolite ATRA in CRC cells supports the involvement of the lncRNA-PLCD4-ATRA axis in CRC pathogenesis. Interestingly, lncRNA 60967.1 and PLCD4 mRNA were found to colocalize in the cytoplasm, and overexpression of lncRNA 60967.1 increased both PLCD4 mRNA and protein levels, suggesting a regulatory role. However, the precise mechanism by which lncRNA 60967.1 modulates PLCD4 expression remains unclear. Given that lncRNAs can influence gene expression through multiple mechanisms—such as altering mRNA stability, modulating translation, or acting as competing endogenous RNAs—further investigation is warranted to elucidate the underlying mechanism [45, 48–50].

PLCD4 encodes phospholipase C delta 4, a member of the phosphoinositide-specific phospholipase C (PLC) family, which hydrolyzes phosphatidylinositol 4,5-bisphosphate into inositol trisphosphate and diacylglycerol, key mediators of calcium signaling, cell proliferation, and differentiation [51–53]. The PLC family consists of 13 isoforms grouped into six subfamilies with distinct regulatory mechanisms and tissue-specific roles [53, 54]. Although research on PLCD4 is limited, mutations in the gene have been observed in 2.18% of cancers, including melanoma, glioblastoma, skin squamous cell carcinoma, and adenocarcinoma of unknown primary origin [55]. Leung et al. demonstrated that PLCD4 overexpression in the MCF7 breast cancer cell line promoted cell proliferation by upregulating ErbB1/2 expression and activating the Erk signaling pathway, suggesting an oncogenic role [56]. In contrast, our data showed that ectopic expression of PLCD4 in CRC cells significantly inhibited their migratory capacity and reduced tumor size in Balb/c nude mice xenografted with PLCD4-overexpressing CRC cells. Similarly, overexpression of lncRNA 60967.1 increased PLCD4 expression, which led to reduced tumor sizes in immunocompetent Balb/c mice injected with CRC cells overexpressing the lncRNA. These findings suggest that PLCD4 functions as a tumor suppressor in CRC but may have an oncogenic role in other cancers like breast cancer. The distinct roles of PLCD4 in various cancer types may be attributed to its involvement in different signaling

pathways. In breast cancer, the DAG generated by PLCD4 overexpression can activate specific PKC isoforms, such as PKC- ϕ . This activation subsequently enhances the transcription of EGFR and ErbB2, leading to the activation of the Erk signaling pathway, which promotes a more proliferative cell growth state [56]. In contrast, reduced PLCD4 expression in CRC likely engages alternative pathways that influence cell growth. For instance, overexpression of PLCD4 in rhabdomyosarcoma (RMS) RD cells upregulates cyclin B1, while knockdown of PLCD4 in A204 RMS cells reduces cyclin B1 expression, suggesting that nuclear PLCD4 regulates cell proliferation via cyclin B1 [57]. Similarly, an independent study demonstrated that PLCD4 knockdown affects cell proliferation and induces senescence in mesenchymal stromal stem cells [58]. However, the precise mechanisms by which PLCD4 functions in CRC remain under intensive investigation.

ATRA is a biologically active derivative of vitamin A and plays a key role in cellular differentiation, growth regulation, and apoptosis by activating retinoic acid receptors [37, 59]. Notably, ATRA is the standard therapy for acute promyelocytic leukemia as a differentiation inducer [60, 61]. While its effectiveness in treating solid tumors remains limited, several studies have demonstrated its anti-tumor effects in thyroid, breast, ovarian, liver, and lung cancers by inhibiting cancer cell proliferation and invasion [62–64]. In this study, we observed reduced ATRA levels in both CRC patients and cell lines. Although overexpression of lncRNA 60967.1 increased ATRA levels, ATRA alone did not impact CRC cell proliferation or apoptosis. However, when combined with IFN- γ stimulation, ATRA significantly inhibited cell growth, suggesting a synergistic effect between ATRA and IFN- γ or a potential role for ATRA in modulating IFN signaling [65–67]. Additionally, ATRA treatment in IFN- γ -resistant CRC cells upregulated IFNGR1 expression (Fig. 4J), a key component of the IFN- γ receptor complex, further supporting ATRA's role in modulating IFN signaling. A recent study confirmed that ATRA restores IFN- γ sensitivity by regulating bisecting N-glycosylation and stabilizing IFN γ Ra [41]. Moreover, downregulation of IFNGR1 in murine CRC cells conferred resistance to anti-PD-1 therapy [68].

Recent studies indicate that ATRA also regulates both the innate and adaptive immune systems, playing a critical role in modulating intestinal immunity [69, 70]. In CRC, microbiota-induced intestinal inflammation disrupts ATRA metabolism, leading to a colonic ATRA deficit that exacerbates carcinogenesis. Conversely, ATRA supplementation has been shown to inhibit cancer progression through a CD8⁺ T cell-dependent mechanism [71]. Consistent with these findings, we observed that ectopic expression of lncRNA 60967.1 upregulates the

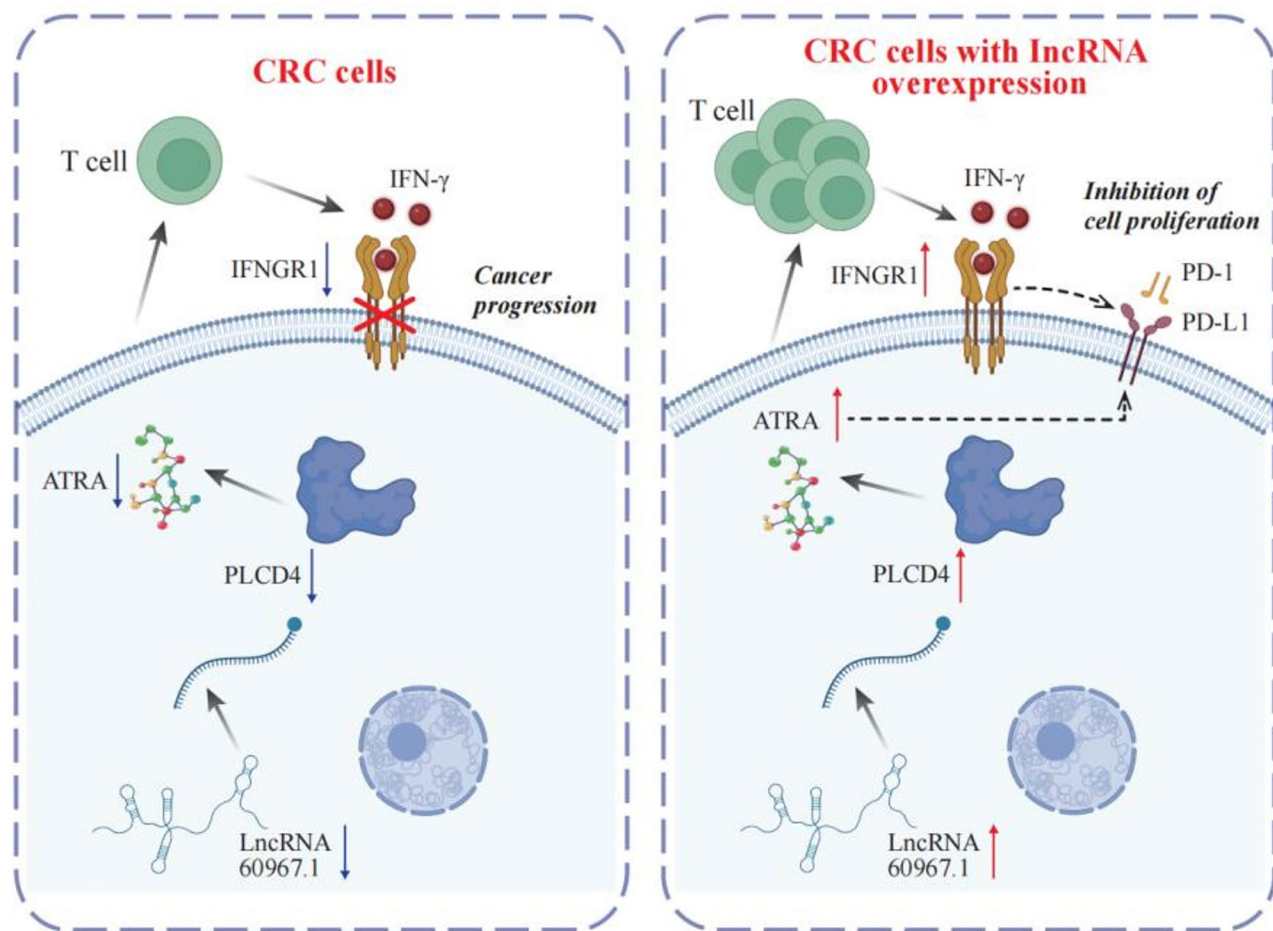


Fig. 8 A proposed model suggests that LncRNA 60967.1 plays a regulatory role in modulating the PLCD4/ATRA axis and anti-PD-1 therapy, influencing immune responses and affecting CRC progression

PLCD4/ATRA axis, resulting in increased infiltration of both CD8⁺ and CD4⁺ T cells and a corresponding reduction in tumor sizes in CRC xenograft models compared to controls. Notably, tumor-infiltrating CD8⁺ T cells are prolific producers of IFN γ , a cytokine critical for antitumor immunity [72, 73]. Given the increased expression of the key IFN γ pathway gene IFNGR1 in CRC xenograft models (Fig. 6), our results suggest that LncRNA 60967.1 suppresses tumor development by modulating tumor microenvironment through ATRA, enhancing immune infiltration, activating IFN γ signaling, and inhibiting tumor proliferation. However, the precise mechanisms by which LncRNA 60967.1 regulates ATRA metabolism and signaling remain to be elucidated and warrant further investigation.

Overexpression of LncRNA 60967.1 significantly enhanced PD-L1 expression in murine CRC cells and synergized with anti-PD-1 therapy to improve tumor control (Fig. 7G), suggesting that LncRNA 60967.1 modulates immune checkpoint pathways and can serve as a promising target for combination immunotherapy (Fig. 8).

Furthermore, knockdown experiments confirmed its regulatory role in immune-related genes (Fig. 7C and D), further underscoring its potential as a key modulator of the tumor microenvironment. Nevertheless, the molecular pathways through which LncRNA 60967.1 governs PD-L1 expression have yet to be fully defined. Whether these effects occur via a single, shared pathway or through multiple distinct signaling axes remains a critical question for future research [48, 74, 75]. Furthermore, LncRNA delivery via viral vectors, lipid-based nanoparticles, or viral-like particles holds potential for improving therapeutic results in cancer treatment [76, 77].

In summary, by analyzing multi-omics data including transcriptomics, proteomics, and metabolomics, we identified a novel regulatory network involving LncRNA, PLCD4, ATRA, and PD-L1 in CRC. The LncRNA 60967.1-PLCD4-ATRA axis plays a role in regulating immune responses and tumor progression in CRC. Overexpression of LncRNA 60967.1 increases PLCD4 expression and ATRA levels, which enhances immune cell infiltration and promotes IFN- γ -induced apoptosis. This

modulation may help reverse immune resistance, particularly in response to immune checkpoint inhibitors like anti-PD-1 therapy. The clinical relevance of this axis lies in its potential to improve treatment outcomes, especially in patients resistant to current therapies. Targeting this axis could serve as a therapeutic strategy to enhance the efficacy of immunotherapy in CRC, and further studies may reveal its utility as a biomarker for treatment response. However, certain limitations must be acknowledged, such as the relatively small sample size and the inability to fully elucidate the regulatory mechanisms among lncRNA 60967.1, PLCD4, ATRA, and PD-L1 due to the complexity of the involved networks [40, 41, 48, 75, 78]. Moreover, a total of 13 patients were enrolled in the study; however, tissue samples from two patients were insufficient for proteomic and metabolomic analysis. Due to limited tissue availability from two patients, the final multi-omics datasets include 26 transcriptomes, 22 proteomes, and 66 metabolomes (triplicates per sample).

Supplementary Information

The online version contains supplementary material available at <https://doi.org/10.1186/s12943-025-02359-x>.

Supplementary Material 1

Supplementary Material 2

Author contributions

SD, NZ, HG, FZ, LX, and YC conceived and designed the study. NZ, YC, LX, YW, XJ, CL, YS, FW, and YL collected samples and performed the experiments. NZ, YC, LX, JH, and XL conducted the data analysis. SD, NZ, HG, XL, YC, and FZ drafted the manuscript. All authors reviewed the manuscript.

Funding

SD is supported by grants from the 2022 Zhejiang Provincial Key R&D Program (No. 2022C03032), the 2023 Provincial-Ministerial Joint Key Project (No. WKJ-ZJ-2313), and the National Natural Science Foundation of China (No. 82072628). HG is supported by the Noncommunicable Chronic Diseases–National Science and Technology Major Project (No. 2024ZD0520100) and the CASHIPS Seed Grant. FZ received the Hundred Talents Program Award from the Chinese Academy of Sciences. LX is supported by the National Natural Science Foundation of China (No. 32200593) and the Natural Science Foundation of Zhejiang Province (No. LQ23H160040).

Data availability

No datasets were generated or analysed during the current study.

Declarations

Ethics approval and consent to participate

The study received ethical approval from Sir Run Run Shaw Hospital, Hangzhou, China. All patients provided written informed consent. The Institutional Animal Care and Use Committee (IACUC) of the respective institutions approved all experiments.

Consent for publication

All the authors have read and approved the final manuscript for publication.

Competing interests

The authors declare no competing interests.

Author details

¹Department of Colorectal Surgery, Sir Run Run Shaw Hospital, School of Medicine, Zhejiang University, Hangzhou, Zhejiang 310016, China

²Provincial Key Laboratory of Precise Diagnosis and Treatment of Abdominal Infection, Sir Run Run Shaw Hospital, School of Medicine, Zhejiang University, Hangzhou, Zhejiang 310016, China

³Anhui Province Key Laboratory of Medical Physics and Technology, Institute of Health and Medical Technology, Hefei Institutes of Physical Science, Chinese Academy of Sciences, Hefei 230031, China

⁴Hefei Cancer Hospital, Chinese Academy of Sciences, Hefei, Anhui Province 230031, China

⁵Hangzhou ShengTing Medical Technology Co., Ltd, Hangzhou, Zhejiang Province 310018, China

Received: 10 February 2025 / Accepted: 19 May 2025

Published online: 06 June 2025

References

1. Morgan E, Arnold M, Gini A, Lorenzoni V, Cabaasag CJ, Laversanne M, Vignat J, Ferlay J, Murphy N, Bray F. Global burden of colorectal cancer in 2020 and 2040: incidence and mortality estimates from GLOBOCAN. *Gut*. 2023;72(2):338–44.
2. Siegel RL, Wagle NS, Cercek A, Smith RA, Jemal A. Colorectal cancer statistics, 2023. *CA Cancer J Clin*. 2023;73(3):233–54.
3. Cancer Genome Atlas N. Comprehensive molecular characterization of human colon and rectal cancer. *Nature*. 2012;487(7407):330–7.
4. Shin AE, Giaccotti FG, Rustgi AK. Metastatic colorectal cancer: mechanisms and emerging therapeutics. *Trends Pharmacol Sci*. 2023;44(4):222–36.
5. Siegel RL, Miller KD, Goding Sauer A, Fedewa SA, Butterly LF, Anderson JC, Cercek A, Smith RA, Jemal A. Colorectal cancer statistics, 2020. *CA Cancer J Clin*. 2020;70(3):145–64.
6. Andrei P, Battuello P, Grasso G, Rovera E, Tesio N, Bardelli A. Integrated approaches for precision oncology in colorectal cancer: the more you know, the better. *Semin Cancer Biol*. 2022;84:199–213.
7. Zhao N, Lai C, Wang Y, Dai S, Gu H. Understanding the role of DNA methylation in colorectal cancer: mechanisms, detection, and clinical significance. *Biochim Biophys Acta Rev Cancer*. 2024;1879(3):189096.
8. Buikhuisen JY, Torang A, Medema JP. Exploring and modelling colon cancer inter-tumour heterogeneity: opportunities and challenges. *Oncogenesis*. 2020;9(7):66.
9. Punt CJ, Koopman M, Vermeulen L. From tumour heterogeneity to advances in precision treatment of colorectal cancer. *Nat Rev Clin Oncol*. 2017;14(4):235–46.
10. Miyamoto Y, Ogawa K, Ohuchi M, Tokunaga R, Baba H. Emerging evidence of immunotherapy for colorectal cancer. *Ann Gastroenterol Surg*. 2023;7(2):216–24.
11. Sahin IH, Ciombor KK, Diaz LA, Yu J, Kim R. Immunotherapy for microsatellite stable colorectal cancers: challenges and novel therapeutic avenues. *Am Soc Clin Oncol Educ Book*. 2022;42:1–12.
12. Karczewski KJ, Snyder MP. Integrative omics for health and disease. *Nat Rev Genet*. 2018;19(5):299–310.
13. Hasin Y, Seldin M, Lusis A. Multi-omics approaches to disease. *Genome Biol*. 2017;18(1):83.
14. Yuan Q, Deng D, Pan C, Ren J, Wei T, Wu Z, Zhang B, Li S, Yin P, Shang D. Integration of transcriptomics, proteomics, and metabolomics data to reveal HER2-associated metabolic heterogeneity in gastric cancer with response to immunotherapy and neoadjuvant chemotherapy. *Front Immunol*. 2022;13:951137.
15. He X, Liu X, Zuo F, Shi H, Jing J. Artificial intelligence-based multi-omics analysis fuels cancer precision medicine. *Semin Cancer Biol*. 2023;88:187–200.
16. Berg KCG, Eide PW, Eilertsen IA, Johannessen B, Bruun J, Danielsen SA, Bjørnslett M, Meza-Zepeda LA, Eknæs M, Lind GE, et al. Multi-omics of 34 colorectal cancer cell lines - a resource for biomedical studies. *Mol Cancer*. 2017;16(1):116.
17. Takei S, Tanaka Y, Lin YT, Koyama S, Fukuoka S, Hara H, Nakamura Y, Kuboki Y, Kotani D, Kojima T et al. Multiomic molecular characterization of the response to combination immunotherapy in MSS/pMMR metastatic colorectal cancer. *J Immunother Cancer* 2024;12(2).
18. Fernandez-Rozadilla C, Timofeeva M, Chen Z, Law P, Thomas M, Schmit S, Díez-Obrero V, Hsu L, Fernandez-Tajes J, Palles C, et al. Author correction:

- Deciphering colorectal cancer genetics through multi-omic analysis of 100,204 cases and 154,587 controls of European and East Asian ancestries. *Nat Genet.* 2023;55(3):519–20.
19. Tomczak K, Czerwińska P, Wiznerowicz M. The Cancer genome atlas (TCGA): an immeasurable source of knowledge. *Contemp Oncol (Pozn).* 2015;19(1a):A68–77.
20. Hutter C, Zenklusen JC. The Cancer genome atlas: creating lasting value beyond its data. *Cell.* 2018;173(2):283–5.
21. Anders S, Huber W. Differential expression analysis for sequence count data. *Genome Biol.* 2010;11(10):R106.
22. Langfelder P, Horvath S. WGCNA: an R package for weighted correlation network analysis. *BMC Bioinformatics.* 2008;9:559.
23. Lyu F, Han F, Ge C, Mao W, Chen L, Hu H, Chen G, Lang Q, Fang C. OmicStudio: A composable bioinformatics cloud platform with real-time feedback that can generate high-quality graphs for publication. *Imeta.* 2023;2(1):e85.
24. Xu Q, Liu X, Liu Z, Zhou Z, Wang Y, Tu J, Li L, Bao H, Yang L, Tu K. MicroRNA-1296 inhibits metastasis and epithelial-mesenchymal transition of hepatocellular carcinoma by targeting SRPK1-mediated PI3K/AKT pathway. *Mol Cancer.* 2017;16(1):103.
25. Meng J, Liu Y, Han J, Tan Q, Chen S, Qiao K, Zhou H, Sun T, Yang C. Hsp90 β promoted endothelial cell-dependent tumor angiogenesis in hepatocellular carcinoma. *Mol Cancer.* 2017;16(1):72.
26. Hanzelmann S, Castelo R, Guinney J. GSEA: gene set variation analysis for microarray and RNA-seq data. *BMC Bioinformatics.* 2013;14:7.
27. Tang Z, Kang B, Li C, Chen T, Zhang Z. GEPIA2: an enhanced web server for large-scale expression profiling and interactive analysis. *Nucleic Acids Res.* 2019;47(W1):W556–60.
28. Li Y, Dou Y, Da Veiga Leprevost F, Geffen Y, Calinawan AP, Aguet F, Akiyama Y, Anand S, Birger C, Cao S, et al. Proteogenomic data and resources for pan-cancer analysis. *Cancer Cell.* 2023;41(8):1397–406.
29. Leng D, Yang Z, Sun H, Song C, Huang C, Ip KU, Chen G, Deng CX, Zhang XD, Zhao Q. Comprehensive analysis of tumor microenvironment reveals prognostic CeRNA network related to immune infiltration in sarcoma. *Clin Cancer Res.* 2023;29(19):3986–4001.
30. Worley B, Powers R. Multivariate analysis in metabolomics. *Curr Metabolomics.* 2013;1(1):92–107.
31. Xia J, Psychogios N, Young N, Wishart DS. MetaboAnalyst: a web server for metabolomic data analysis and interpretation. *Nucleic Acids Res.* 2009;37(Web Server issue):W652–660.
32. Parks DH, Beiko RG. Identifying biologically relevant differences between metagenomic communities. *Bioinformatics.* 2010;26(6):715–21.
33. Rhee SG, Bae YS. Regulation of phosphoinositide-specific phospholipase C isozymes. *J Biol Chem.* 1997;272(24):15045–8.
34. Hill TD, Dean NM, Boynton AL. Inositol 1,3,4,5-tetrakisphosphate induces Ca²⁺ + sequestration in rat liver cells. *Science.* 1988;242(4882):1176–8.
35. Lim PS, Sutton CR, Rao S. Protein kinase C in the immune system: from signaling to chromatin regulation. *Immunology.* 2015;146(4):508–22.
36. Jette C, Peterson PW, Sandoval IT, Manos EJ, Hadley E, Ireland CM, Jones DA. The tumor suppressor adenomatous polyposis coli and caudal related homeodomain protein regulate expression of retinol dehydrogenase L. *J Biol Chem.* 2004;279(33):34397–405.
37. Kropotova ES, Zinovieva OL, Zyryanova AF, Dybova VI, Prasolov VS, Beresten SF, Oparina NY, Mashkova TD. Altered expression of multiple genes involved in retinoic acid biosynthesis in human colorectal cancer. *Pathol Oncol Res.* 2014;20(3):707–17.
38. Giulì MV, Hanieh PN, Giuliani E, Rinaldi F, Marianecci C, Screpanti I, Checquolo S, Carafa M. Current trends in ATRA delivery for Cancer therapy. *Pharmaceutics* 2020;12(8).
39. Kam RK, Deng Y, Chen Y, Zhao H. Retinoic acid synthesis and functions in early embryonic development. *Cell Biosci.* 2012;2(1):11.
40. Bi G, Liang J, Bian Y, Shan G, Besskaya V, Wang Q, Zhan C. The Immunomodulatory role of all-trans retinoic acid in tumor microenvironment. *Clin Exp Med.* 2023;23(3):591–606.
41. Krug J, Rodrian G, Petter K, Yang H, Khoziainova S, Guo W, Bénard A, Merkel S, Gellert S, Maschauer S, et al. N-glycosylation regulates intrinsic IFN- γ resistance in colorectal cancer: implications for immunotherapy. *Gastroenterology.* 2023;164(3):392–e406395.
42. DeCicco KL, Youngdahl JD, Ross AC. All-trans-retinoic acid and polyribonucleosinic: polyribocytidylic acid in combination potentiate specific antibody production and cell-mediated immunity. *Immunology.* 2001;104(3):341–8.
43. Chelbi-Alix MK, Pelicano L. Retinoic acid and interferon signaling cross talk in normal and RA-resistant APL cells. *Leukemia.* 1999;13(8):1167–74.
44. Garattini E, Mologni L, Ponzanelli I, Terao M. Cross-talk between retinoic acid and interferons: molecular mechanisms of interaction in acute promyelocytic leukemia cells. *Leuk Lymphoma.* 1998;30(5–6):467–75.
45. Mattick JS, Amaral PP, Carninci P, Carpenter S, Chang HY, Chen LL, Chen R, Dean C, Dinger ME, Fitzgerald KA, et al. Long non-coding RNAs: definitions, functions, challenges and recommendations. *Nat Rev Mol Cell Biol.* 2023;24(6):430–47.
46. Zhang B, Wang J, Wang X, Zhu J, Liu Q, Shi Z, Chambers MC, Zimmerman LJ, Shaddox KF, Kim S, et al. Proteogenomic characterization of human colon and rectal cancer. *Nature.* 2014;513(7518):382–7.
47. Mukherjee A, Chiang CY, Daifotis HA, Nieman KM, Fahrman JF, Lastra RR, Romero IL, Fiehn O, Lengyel E. Adipocyte-Induced FABP4 expression in ovarian Cancer cells promotes metastasis and mediates carboplatin resistance. *Cancer Res.* 2020;80(8):1748–61.
48. Schmitt AM, Chang HY. Long noncoding RNAs in Cancer pathways. *Cancer Cell.* 2016;29(4):452–63.
49. Yu J, Zhang Y, Xue Y, Pei H, Li B. Emerging roles of long noncoding RNAs in enzymes related intracellular metabolic pathways in cancer biology. *Biomed Pharmacother.* 2024;176:116831.
50. De Martino M, Esposito F, Pallante P. Long non-coding RNAs regulating multiple proliferative pathways in cancer cell. *Transl Cancer Res.* 2021;10(6):3140–57.
51. Rhee SG. Regulation of phosphoinositide-specific phospholipase C. *Annu Rev Biochem.* 2001;70:281–312.
52. Rebecchi MJ, Pentyala SN. Structure, function, and control of phosphoinositide-specific phospholipase C. *Physiol Rev.* 2000;80(4):1291–335.
53. Williams RL. Mammalian phosphoinositide-specific phospholipase C. *Biochim Biophys Acta.* 1999;1441(2–3):255–67.
54. Gresset A, Sondek J, Harden TK. The phospholipase C isozymes and their regulation. *Subcell Biochem.* 2012;58:61–94.
55. Consortium APG. AACR project GENIE: powering precision medicine through an international consortium. *Cancer Discov.* 2017;7(8):818–31.
56. Leung DW, Tompkins C, Brewer J, Ball A, Coon M, Morris V, Waggoner D, Singer JW. Phospholipase C delta-4 overexpression upregulates ErbB1/2 expression, Erk signaling pathway, and proliferation in MCF-7 cells. *Mol Cancer.* 2004;3:15.
57. Salucci S, Bavelloni A, Versari I, Burattini S, Bavelloni F, Gobbi P, Panzani A, Codenotti S, Blalock W, Scotlandi K et al. Phospholipase C δ -4 (PLC δ 4) acts as a nuclear player to influence Cyclin B expression in the embryonal rhabdomyosarcoma cell lines RD and A204. *Biomolecules* 2024;14(9).
58. Kunrath-Lima M, de Miranda MC, Ferreira ADF, Faraco CCF, de Melo MIA, Goes AM, Rodrigues MA, Faria J, Gomes DA. Phospholipase C delta 4 (PLC δ 4) is a nuclear protein involved in cell proliferation and senescence in mesenchymal stromal stem cells. *Cell Signal.* 2018;49:59–67.
59. Brown G. Targeting the retinoic acid pathway to eradicate Cancer stem cells. *Int J Mol Sci* 2023;24(3).
60. Lo-Coco F, Avvisati G, Vignetti M, Thiede C, Orlando SM, Iacobelli S, Ferrara F, Fazi P, Cicconi L, Di Bona E, et al. Retinoic acid and arsenic trioxide for acute promyelocytic leukemia. *N Engl J Med.* 2013;369(2):111–21.
61. Chlapek P, Slavikova V, Mazanek P, Sterba J, Veselska R. Why differentiation therapy sometimes fails: molecular mechanisms of resistance to retinoids. *Int J Mol Sci* 2018;19(1).
62. Schenk T, Stengel S, Zelent A. Unlocking the potential of retinoic acid in anticancer therapy. *Br J Cancer.* 2014;111(11):2039–45.
63. Erkelens MN, Mebius RE. Retinoic acid and immune homeostasis: A balancing act. *Trends Immunol.* 2017;38(3):168–80.
64. Lokman NA, Ho R, Gunasegaran K, Bonner WM, Oehler MK, Ricciardelli C. Anti-tumour effects of all-trans retinoid acid on serous ovarian cancer. *J Exp Clin Cancer Res.* 2019;38(1):10.
65. Pelicano L, Li F, Schindler C, Chelbi-Alix MK. Retinoic acid enhances the expression of interferon-induced proteins: evidence for multiple mechanisms of action. *Oncogene.* 1997;15(19):2349–59.
66. Percario ZA, Giandomenico V, Fiorucci G, Chiantore MV, Vannucchi S, Hiscott J, Affabris E, Romeo G. Retinoic acid is able to induce interferon regulatory factor 1 in squamous carcinoma cells via a STAT-1 independent signalling pathway. *Cell Growth Differ.* 1999;10(4):263–70.
67. Matikainen S, Ronni T, Lehtonen A, Sareneva T, Melen K, Nordling S, Levy DE, Julkunen I. Retinoic acid induces signal transducer and activator of transcription (STAT) 1, STAT2, and p48 expression in myeloid leukemia cells and enhances their responsiveness to interferons. *Cell Growth Differ.* 1997;8(6):687–98.

68. Lv C, Yuan D, Cao Y. Downregulation of Interferon-gamma receptor expression endows resistance to Anti-Programmed death protein 1 therapy in colorectal Cancer. *J Pharmacol Exp Ther*. 2021;376(1):21–8.
69. Cassani B, Villablanca EJ, De Calisto J, Wang S, Mora JR. Vitamin A and immune regulation: role of retinoic acid in gut-associated dendritic cell education, immune protection and tolerance. *Mol Aspects Med*. 2012;33(1):63–76.
70. Hall JA, Grainger JR, Spencer SP, Belkaid Y. The role of retinoic acid in tolerance and immunity. *Immunity*. 2011;35(1):13–22.
71. Bhattacharya N, Yuan R, Prestwood TR, Penny HL, DiMaio MA, Reticker-Flynn NE, Krois CR, Kenkel JA, Pham TD, Carmi Y, et al. Normalizing Microbiota-Induced retinoic acid deficiency stimulates protective CD8(+) T Cell-Mediated immunity in colorectal Cancer. *Immunity*. 2016;45(3):641–55.
72. Farhood B, Najafi M, Mortezaee K. CD8(+) cytotoxic T lymphocytes in cancer immunotherapy: A review. *J Cell Physiol*. 2019;234(6):8509–21.
73. Komita H, Homma S, Saotome H, Zeniya M, Ohno T, Toda G. Interferon-gamma produced by interleukin-12-activated tumor infiltrating CD8+T cells directly induces apoptosis of mouse hepatocellular carcinoma. *J Hepatol*. 2006;45(5):662–72.
74. Chen L, Han X. Anti-PD-1/PD-L1 therapy of human cancer: past, present, and future. *J Clin Invest*. 2015;125(9):3384–91.
75. Peng WX, Koirala P, Mo YY. LncRNA-mediated regulation of cell signaling in cancer. *Oncogene*. 2017;36(41):5661–7.
76. Raguram A, Banskota S, Liu DR. Therapeutic in vivo delivery of gene editing agents. *Cell*. 2022;185(15):2806–27.
77. Kaczmarek JC, Kowalski PS, Anderson DG. Advances in the delivery of RNA therapeutics: from concept to clinical reality. *Genome Med*. 2017;9(1):60.
78. Kunrath-Lima M, de Miranda MC, Ferreira ADF, Faraco CCF, de Melo MIA, Goes AM, Rodrigues MA, Faria J, Gomes DA. Phospholipase C delta 4 (PLCdelta4) is a nuclear protein involved in cell proliferation and senescence in mesenchymal stromal stem cells. *Cell Signal*. 2018;49:59–67.

Publisher's note

Springer Nature remains neutral with regard to jurisdictional claims in published maps and institutional affiliations.